# Direct neuronal conversion of microglia/macrophages reinstates neurological function after stroke

Takashi Irie[1,2], Taito Matsuda[1]*, Yoshinori Hayashi[3], Akihide Kamiya[4,5], Jun-ichi Kira[2], Kinichi Nakashima[1]*

## Abstract

Ischaemic brain injury causes permanent neuronal loss, which often results in persistent severe neurological dysfunctions. Although generating new neurons in the injured brain would be an ideal approach to replenish the lost neurons for repairing the damage, the adult mammalian brain retains only limited neurogenic capability. Here, we show that direct conversion of microglia/macrophages into neurons in the brain has great potential as a therapeutic strategy for ischaemic brain injury. After transient middle cerebral artery occlusion in adult mice, microglia/macrophages converge at the lesion core of the striatum, where neuronal loss is prominent. Targeted expression of a neurogenic transcription factor, NeuroD1, in microglia/macrophages in the injured striatum enables their conversion into induced neuronal cells that functionally integrate into the existing neuronal circuits. Furthermore, NeuroD1-mediated induced neuronal cell generation significantly improves neurological function in the mouse stroke model, and

ablation of these cells abolishes the gained functional recovery. Our findings thus demonstrate that neuronal conversion contributes directly to functional recovery after stroke and shed further light on the development of therapies for ischaemic brain injury by *in situ* neuronal conversion technology.

**Affiliations:**

[1]Department of Stem Cell Biology and Medicine, Graduate School of Medical Sciences, Kyushu University, Fukuoka, Japan.

[2]Department of Neurology, Neurological Institute, Graduate School of Medical Sciences, Kyushu University, Fukuoka, Japan.

[3]Department of Physiology, Nihon University School of Dentistry, Tokyo, Japan.

[4]Department of Molecular Life Sciences, Tokai University School of Medicine, Isehara, Japan.

[5]Center for Stem Cell Biology and Regenerative Medicine, Institute of Medical Science, University of Tokyo, Tokyo, Japan.

* CORRESPONDENCE TO:

Taito Matsuda,

Department of Stem Cell Biology and Medicine,

Graduate School of Medical Sciences, Kyushu University,

3-1-1, Maidashi, Higashi-ku, Fukuoka 812-8582, Japan.

Phone: +81-92-642-6196; E-mail: tmatsuda@scb.med.kyushu-u.ac.jp

Kinichi Nakashima,

Department of Stem Cell Biology and Medicine,

Graduate School of Medical Sciences, Kyushu University,

3-1-1, Maidashi, Higashi-ku, Fukuoka 812-8582, Japan.

Phone: +81-92-642-6195; E-mail: kin1@scb.med.kyushu-u.ac.jp

**Running title:** Direct neuronal conversion after stroke

**Keywords:** direct reprogramming; microglia; NeuroD1; neurogenesis; stroke

**Abbreviations:** DT = diphtheria toxin; iDTR = inducible diphtheria toxin receptor; iN = induced neuronal; MCA = middle cerebral artery; ND1 = NeuroD1; NS/PC = neural stem/precursor cell; SPN = striatal projection neuron; SVZ = subventricular zone; TH =

tyrosine hydroxylase; tMCAO = transient middle cerebral artery occlusion; wpi = week(s) post-injection

# Introduction

Stroke is often associated with severe disabilities, high recurrence rate, and other poor outcomes. Since neuronal loss is a major pathological hallmark of brain injury, regenerating new neurons to replenish lost neurons in the injured area is critical for functional recovery. A novel approach towards achieving the replacement of damaged neurons is to induce *in vivo* fate conversion of non-neuronal cells residing within the injured brain into neurons. Several groups have achieved *in vivo* fate conversion within the mouse brain by instructing endogenous astrocytes or oligodendrocyte progenitor cells to generate induced neuronal (iN) cells.[1-7] Moreover, a recent study has shown the conversion of astrocytes to iN cells in a focal ischaemia model induced by the vasoconstrictive peptide endothelin-1, resulting in the improvement of some neurological dysfunctions.[8] However, most thromboembolic infarcts in humans occur in the territory of the middle cerebral artery (MCA),[9] and transient MCA occlusion (tMCAO) induces massive loss of astrocytes as well as neurons in the injured area,[10] which makes it difficult to target astrocytes for neuronal reprogramming in this context. Thus, it is important to assess the effect of iN cell generation by targeting non-neuronal cells residing within the injured area other than astrocytes using a tMCAO model. Furthermore, it has yet to be shown whether the iN cells participate directly in functional recovery following brain

injury, which is an outstanding critical question to be solved before we can move forward to clinical application using this *in situ* neuronal conversion technology.

Microglia are CNS-resident macrophages and are derived from primitive macrophages,[11] which arise from early erythro-myeloid progenitors in the yolk sac during the early embryonic stage.[12-14] With the establishment of the blood circulation, these primitive macrophages migrate into the developing CNS, and a combination of ontogeny and CNS environment confers the microglial signature on the migrated cells.[15-17] Although microglia maintain their CNS population by self-renewal in the normal brain, CNS injury prompts peripheral macrophages to infiltrate into the brain by passing through a disrupted blood-brain barrier. CNS-infiltrated macrophages initially retain peripheral identity, but they eventually acquire a highly similar gene expression pattern to that of brain-resident microglia and act similarly to microglia after injury.[18, 19]

In response to ischaemic stroke within the MCA, although astrocytes become reactive and form an astrocytic scar in the peri-injured region, microglia/macrophages converge more internally within the area of insult, i.e., in the lesion core, where neuronal loss is prominent.[10, 20-24] Since microglia as well as macrophages regenerate rapidly,[25] microglia/macrophages that converge at the lesion core should be an ideal target for direct conversion to replenish lost neurons after brain injury without exhaustion of their source

in the brain. We have previously revealed that a single transcription factor, NeuroD1 (ND1), directly converts microglia into neurons both *in vitro* and in the mouse adult brain under normal conditions.[26] Here, we report that ND1 can convert microglia/macrophages into iN cells in the injured striatum of tMCAO mice. ND1-converted iN cells expressed a marker for striatal projection neurons (SPNs) and were functionally integrated into the existing brain circuits in the ischaemic area. In addition, iN cell-specific ablation abolished the restored neurological function in tMCAO mice, indicating that iN cells make a direct and major contribution to the attained functional recovery after ischaemic injury.

# Materials and methods

## Mice

All efforts were made to minimize animal suffering and to reduce the number of animals used. Animals were housed under a 12/12-h light/dark cycle and fed *ad libitum*. Male 8-week-old wild-type mice (C57BL/6, obtained from Japan SLC), Nestin-Cre$^{ERT2}$::Stop-EGFP (a generous gift from Dr. I. Imayoshi), and iDTR mice (purchased from the Jackson Laboratory) were used for a mouse model of ischaemic stroke. All experiments were carried out according to the animal experimentation guidelines of Kyushu University,

Tokai University or University of Tokyo, which comply with the National Institutes of Health Guide for the Care and Use of Laboratory Animals.

## Mouse model of ischaemic stroke

Transient middle cerebral artery occlusion (tMCAO) was performed as described previously.[27, 28] Briefly, 8-week-old mice were anaesthetized with a mixture of 4 mg/kg midazolam, 0.3 mg/kg medetomidine, and 5 mg/kg butorphanol, and tMCAO was generated by the insertion of a silicon-coated monofilament (6-0 medium MCAO suture L34 No. 602334, Doccol Corporation) *via* the right proximal external carotid artery into the internal carotid artery. The distance from the suture tip to the right common carotid artery bifurcation was 9–10 mm. Thirty minutes after the right tMCAO, the inserted monofilament was withdrawn to allow reperfusion. After the operation, the effects of medetomidine were reversed with atipamezole. Mice that displayed more than 80% of biased swing behaviour in the elevated body swing test and more than 80% of biased turning behaviour in the corner test at 1 week after tMCAO were used as tMCAO mice in this study. For sham group animals, vessels were visualized and cleared of overlying connective tissue as would be done in normal surgical dissection, but no additional manipulations were made. The operator assigned numbers to mice at random, and

assessed behavioural testing by managing the numbers to be blind to the treatments during the testing.

## Behavioural testing

**Elevated body swing test.** By the base of the tail, the mouse was elevated to approximately 10 cm from the bottom of the cage and the direction of the first body swing, more than 10° bending of the upper body from the vertical axis to either side, was recorded.[29] The procedure was repeated 20 times. The laterality index was computed as follows: [Swings (left)] / [Swings (left) + Swings (right)]. The experimenter was blinded to treatment group throughout behavioural testing. Other investigators blinded to the treatments also checked the videos of behavioural testing.

**Corner test.** A modified version of the corner test was used.[30] The testing apparatus consisted of four connecting board walls joined at 30° and 150° angles. To start the trial, animals were placed halfway in and facing a corner. When the mouse entered the deep part of the corner, both sides of the vibrissae were stimulated together by the two boards. In response the mouse reared forward and upward, and then turned back to face the open end. Ten trials were performed for each mouse and the percentage of right turns was calculated. Only turns involving full rearing along either board were recorded.

Occasional turns that did not involve the initial rearing motion were not counted. The laterality index was computed as follows: [Turns (right)] / [Turns (left) + Turns (right)]. The experimenter was blinded to treatment group throughout behavioural testing. Other investigators blinded to the treatments also checked the videos of behavioural testing.

**Corner rotation.** To quantify turning behaviour independently from the strict rearing and turning paradigm used in the corner test, every complete 180° turn to the left or right with or without rearing during the first 5 min of the corner test was scored.[30] Incomplete turns were ignored. The laterality index was computed as follows: [Turns (right)] / [Turns (left) + Turns (right)]. The experimenter was blinded to treatment group throughout behavioural testing. Other investigators blinded to the treatments also checked the videos of behavioural testing.

**Cylinder test.** The mouse was placed in a transparent cylinder 9 cm in diameter and 15 cm in height and videotaped during the test.[31] A mirror was placed at an angle behind the cylinder to enable the rater to record forelimb movements when the mouse was turned away from the camera. After the mouse was put into the cylinder, forelimb use in the first contact against the wall after rearing and during lateral exploration was recorded by the following criteria. (i) The first forelimb to contact the wall during a full rear was recorded as an independent wall placement for that limb. (ii) Simultaneous use

of both the left and right forelimb by contacting the wall of the cylinder during a full rear and for lateral movements along the wall was recorded as ‘‘both’’ movement. (iii) After the first forelimb (for example, the right forelimb) contacted the wall and then the other forelimb was placed on the wall, but the right forelimb was not removed from the wall, a ‘‘right forelimb independent’’ movement and a ‘‘both’’ movement were recorded. However, if the other (left) forelimb made several contacting movements on the wall, a ‘‘right forelimb independent’’ movement and only one ‘‘both’’ movement were recorded. (iv) When the mouse explored the wall laterally, alternating both forelimbs, it was recorded as a ‘‘both’’ movement. A total of 20 movements were recorded during the 10-min test. The laterality index was calculated as follows: [Contacts (right) – Contacts (left)] / [Contacts (left) + Contacts (right) + Contacts (both)]. The experimenter was blinded to treatment group throughout behavioural testing. Other investigators blinded to the treatments also checked the videos of behavioural testing.

## iN cell induction

To induce iN cells, we used lentiviral vectors in which gene expression is controlled under the human *CD68* promoter. The human *CD68* promoter[32] was cloned into the lentiviral vector FG12 (Addgene) using XbaI and XhoI sites. ND1–P2A was then replaced with the

*UbiC* promoter using XhoI and AgeI sites. Cre or tdTomato were cloned and replaced with EGFP using AgeI and BsrgI sites, respectively. Lentiviruses were produced by transfecting HEK293T cells with the lentivirus constructs pCMV–VSV–G–RSV–Rev and pCAG–HIVgp using polyethylenimine. Culture supernatants containing lentivirus were collected 48 h after transfection and centrifuged at 6,000*g* overnight at 4°C. The virus was concentrated using Lenti-X Concentrator (Clontech), and suspended in PBS.

## Stereotactic brain injections

Striata of adult mice were stereotactically injected with 2.0 µl virus with a titer of 0.5 – 2 × $10^9$ particles per milliliter. Injection coordinates were as follows: anterior/posterior, +0.8 mm; medial/lateral, ±2.0 mm; and dorsal/ventral from skull, −3.0 mm.

To label iN cells projected into the globus pallidus, 0.3 µl of Alexa Fluor 488-conjugated CTB (Invitrogen, C34775) was injected into the globus pallidus of iDTR tMCAO model mice at 10 weeks after CD68–ND1–P2A–Cre lentivirus injection. Injection coordinates were as follows: anterior/posterior, −0.5 mm; medial/lateral, ±1.9 mm; and dorsal/ventral from skull, −4.0 mm. Five days later, the animals were fixed.

## Microglial ablation

For the ablation of brain microglia, mice were fed with PLX5622-formulated D12450J diet (12 mg PLX5622 per kg of diet, Research Diets) *ad libitum* during 5 weeks.

## Tamoxifen administration

Tamoxifen (Sigma-Aldrich, T5648) was dissolved in sesame oil at 25 mg/ml. For tamoxifen-inducible Cre-mediated EGFP expression, 10 mg of tamoxifen was orally administered to 6-week-old Nestin–Cre$^{ERT2}$::Stop–EGFP mice for four consecutive days.

## Ablation of iN cells

Since mouse cells are much less sensitive to diphtheria toxin (DT) than human cells, we could ablate only Cre-transduced cells in the inducible DT receptor (iDTR) mouse by injecting DT. DT (FUJIFILM Wako Pure Chemical Corporation) was diluted in PBS (5 μg/ml). Two or six weeks after viral injection, 1 μg of toxin or 0.2 ml of PBS was given by intraperitoneal injection for three consecutive days. To detect DTR expression, we used an anti-human heparin-binding EGF-like growth factor (HBEGF) antibody.

## Immunohistochemistry

Adult mouse brains were fixed in 4% paraformaldehyde, and 40-μm sections were cut

with a cryostat (Leica). Cryosections were washed with PBS and blocked for 1 h at room temperature (RT) with blocking solution (5% FBS, 0.3% Triton X-100), and incubated overnight at 4°C with primary antibodies diluted in blocking solution. The following primary antibodies were used in this study: rabbit anti-Tmem119 (1:200, ab209064; Abcam), goat anti-Iba1 (1:500, ab5076; Abcam), rabbit anti-Iba1 (1:500, 019-19741; FUJIFILM Wako Pure Chemical Corporation), rabbit anti-βIII-tubulin (1:500, PRB-435P; Covance), mouse anti-Map2ab (1:500, M1406; Sigma), mouse anti-NeuN (1:500, MAB377; Merck Millipore), rabbit anti-DARPP32 (1:500, ab40801; Abcam), chick anti-GFAP (1:500, AB5541; Merck Millipore), rabbit anti-GFAP (1:500, G9269; Sigma), mouse anti-APC (1:1000, OP80; Calbiochem), chick anti-GFP (1:500, GFP-1010; Aves Laboratories), rat anti-RFP (1:500, RFP 5F8; ChromoTek), goat anti-HBEGF (1:200, AF259; R&D Systems), mouse anti-HBEGF (1:500, 013-27191; FUJIFILM Wako Pure Chemical Corporation), rabbit anti-Ki67 (1:500, ab15580; Abcam), chick anti-tyrosine hydroxylase (1:1000, TYH; Aves Laboratories), rabbit anti-calretinin (1:500, AB5054; Merck Millipore), rat anti-Ctip2 (1:500, ab18465; Abcam) and rabbit anti-Cux1 (1:100, ABE217; Merck Millipore). Nuclei were stained using Hoechst 33258 (Nacalai Tesque). Stained sections were visualized with a confocal microscope (LSM800, Zeiss).

## Evaluation of cell number and area

Marker-positive cell number in the striatum was quantified using every 6th hemisphere section. The number of marker-positive cells was counted and multiplied by 6 to estimate the total number. The infarct area in the striatum was detected by DARPP32 staining and measured using ImageJ software (National Institutes of Health) and ZEN lite (Zeiss). The infection rate of microglia/macrophages following the virus injection in the striatum shows the proportion of Iba1- and DTR-positive cells at 1 wpi (week(s) post-injection) among Iba1-positive cells at 7 days after MCAO. The total number of Iba1-positive cells at 7 days after MCAO was estimated from cell density multiplied by total area where Iba1-positive cells in the striatum accumulated. The neuronal conversion rate shows the proportion of DARPP32- and DTR-positive cells at 8 wpi among Iba1- and DTR-positive cells at 1 wpi. The ablation rate of iN cells following DT administration shows the proportion of DARPP32- and DTR-positive cells at 8 wpi following DT administration in the virus-injected area of the striatum compared with PBS administration.

## Electrophysiology

For *ex vivo* electrophysiology, striatum slices were cut into 200-μm-thick sections with a VT1000 vibratome (Leica) using ice-cold cutting solution consisting of (in mM) 234

sucrose, 2.5 KCl, 1.25 $NaH_2PO_4$, 10 $MgCl_2$, 0.5 $CaCl_2$, 25 $NaHCO_3$, 11 glucose and 0.5 myoinositol. Whole-cell patch-clamp recording was performed in voltage-clamp mode on EGFP-positive cells according to a similar method described previously.[33] Signals were recorded using a patch-clamp amplifier (Axopatch200B; Molecular Devices). The external solution consisted of (in mM) 125 NaCl, 2.5 KCl, 1.25 $NaH_2PO_4$, 2 $MgCl_2$, 1.6 $CaCl_2$, 10 glucose and 25 $NaHCO_3$ saturated with 95% $O_2$ and 5% $CO_2$. Patch pipettes (8–10 MΩ) were filled with an internal solution of (in mM) 120 K-gluconate, 10 HEPES, 0.2 EGTA, 20 KCl, 2 $MgCl_2$, 7 $Na_2$-phosphocreatine, 4 Mg-ATP and 0.3 $Na_2$-GTP, pH adjusted to 7.3 with KOH. Spontaneous excitatory postsynaptic currents (EPSCs) and inhibitory postsynaptic currents (IPSCs) were recorded at a holding potential of −70 mV and 0 mV, respectively, in the presence 10 μM bicuculline methiodide (a $GABA_A$ receptor antagonist). The evoked action potentials were recorded in current-clamp mode. Current steps (0–120 pA, increasing in increments of 10 pA) were applied for 500 ms. The spontaneous EPSCs, IPSCs and evoked action potentials were analysed by Mini Analysis Program (Synaptosoft) and Clampfit (Molecular Devices). For biocytin labelling, intracellular solution was supplemented with 0.3% biocytin (Vector Laboratories, SP-1120).

# Quantification and statistical analysis

No statistical methods were used to pre-determine sample sizes. Statistical analyses were done afterwards without interim data analysis. No data points were excluded. We did not use any methods to determine whether the data met assumptions of the statistical approach. All data were collected and processed randomly. A two-tailed Mann-Whitney U test was used to calculate the *P* value for pairwise comparisons. For multiple comparisons, *P* values were calculated using 2-way repeated-measures ANOVA and *post hoc* Bonferroni's multiple comparison test. The values of *n* (sample size) are provided in the Figures and Figure legends. We considered a *P* value less than 0.05 to be statistically significant. Data represent mean ± SEM.

# Study approval

All experiments were carried out according to the animal experimentation guidelines of Kyushu University, Tokai University School of Medicine or University of Tokyo, which comply with the National Institutes of Health Guide for the Care and Use of Laboratory Animals.

# Data availability

The data presented in this study are available from the corresponding authors upon request.

# Results

## Microglia/macrophages accumulate at the ischaemic core after tMCAO

We first examined the condition of the lesion site induced by 30 min of right tMCAO, using immunohistochemistry. The brain damage is largely restricted to the striatum after 30 min of tMCAO in mice.[10, 30, 34] Consistent with these reports, we observed considerable loss of DARPP32-positive SPNs in the striatum at 7 days after tMCAO and also found that cells positive for Iba1 (a marker for both microglia and peripheral macrophages) converged in the lesion core (Supplementary Fig. 1A). By contrast, GFAP-positive astrocytes resided in the peri-infarct area and surrounded Iba1-positive cells in the core region (Supplementary Fig. 1A), in agreement with previous studies.[10, 22, 23] Next, we checked the spatiotemporal distribution of microglia/macrophages in the injured striatum after tMCAO by chronological immunohistochemistry using an additional antibody for microglia, Tmem119,[18, 35] which is also expressed in microglia-like cells derived from peripheral macrophages but not in peripheral macrophages themselves. Although only a small number of Iba1/Tmem119-

double-positive cells were observed in the injured region at day 3 after tMCAO, these cells dramatically increased in number by day 7 and were sustained at day 10 (Supplementary Fig. 1B and C). We also detected cells displaying sustained peripheral macrophage-type marker expression (Iba1-positive and Tmem119-negative) in the injured region by day 10, and these cells were virtually absent at day 28 (Supplementary Fig. 1B and C).

## ND1 converts microglia/macrophages to iN cells in the ischaemic region

Having observed accumulation of microglia/macrophages in the lesion core after tMCAO, we then assessed whether ND1 can induce neuronal conversion from these cells. To this end, we employed a lentivirus, used previously to induce microglia-to-neuron conversion in the intact brain,[26] expressing ND1–P2A–EGFP under the promoter of *CD68*, a gene expressed in the inactive state of microglia/macrophages[32] and further upregulated after tMCAO.[18] We injected control or CD68–ND1–P2A–EGFP virus into the ischaemic area at 1 week after tMCAO, when microglia/macrophages greatly accumulate (Supplementary Fig. 1B and C). Two wpi in tMCAO mice, microglia-type cells (Tmem119/Iba1-double-positive) rather than peripheral macrophage-type cells

(Tmem119-negative and Iba1-positive) became predominant in the injured area (Supplementary Fig. 2A and B), and over 80% of the control virus-infected cells were microglia-type cells (Fig. 1A). We also found that very few ND1-transduced cells were microglia-type cells at 2 wpi (Supplementary Fig. 2C and Fig. 1A), implying that they had already begun to be reprogrammed into iN cells. In addition, only a small percentage of control and ND1-expressing virus-infected cells were GFAP-positive astrocytes and APC-positive oligodendrocytes, and almost no change in the ratio was observed between cells infected with control and ND1-expressing viruses (Supplementary Fig. 2D and E, and Fig. 1A). In contrast, similar to the case of intact brain,[26] we found that approximately 60% and 30% of ND1-transduced cells were positive for βIII-tubulin and Map2ab, respectively (Fig. 1B–D, and Supplementary Fig. 2F and G), suggesting that ND1-transduced cells turned into iN cells, partially if not completely, by 2 wpi in the injured striatum. Moreover, when we depleted microglia-type cells (Tmem119/Iba1-double-positive) from the brain by feeding mice with PLX5622 (PLX)-formulated diet continuously from 2 weeks prior to tMCAO and until the mice were sacrificed (Fig. 1E and F), the appearance of ND1-converted Map2ab-positive iN cells was virtually abolished in the ischaemic area (Fig. 1G and H) although peripheral macrophage-type cells (Tmem119-negative and Iba1-positive) remained present in PLX-treated tMCAO

mouse striatum and their number was higher than in PLX-untreated tMCAO mouse striatum (Supplementary Fig. 2C, H and I), in agreement with a previous study.[36] Taking these observations together with the knowledge that PLX (a CSF1R inhibitor) specifically ablates microglia but not peripheral macrophages[36, 37] (Fig. 1F and Supplementary Fig. 2C, H and I), it is conceivable that the majority of original cells converted into iN cells by CD68–ND1–P2A–EGFP virus were microglia-type cells composed of resident microglia and microglia-like cells derived from peripheral macrophages in the ischaemic brain, although it remains unclear whether either or both cell populations were actually converted into iN cells.

We also asked whether neuronal conversion from microglia-type cells reduces their number in the injured region. Although the number of microglia-type cells decreased in the core of the virus-infected region of ND1 virus-injected tMCAO mice at 2 wpi compared with control, there was no significant difference in the periphery of the virus-infected region between them (Supplementary Fig. 2J).

## Neural stem/precursor cells in the subventricular zone are not the origin of iN cells

In the ischemic brain, it has been reported that a limited population of new

neurons derived from neural stem/precursor cells (NS/PCs) in the subventricular zone (SVZ) migrate toward the injured site.[38] To exclude the possibility that a subpopulation of ND1-converted iN cells originate from such NS/PCs, we crossed Nestin-Cre$^{ERT2}$ mice with Stop-EGFP mice and administered their offspring with tamoxifen orally before tMCAO surgery to permanently label Nestin-positive NS/PCs and their progeny (Supplementary Fig. 3A). EGFP-positive cells appeared in the SVZ after tMCAO, but no tdTomato-positive iN cells induced by CD68–ND1–P2A–tdT virus in the ischaemic area were positive for EGFP (Supplementary Fig. 3B–D), indicating that NS/PCs could not be the source of iN cells converted by ND1 expression in this experimental setting.

## ND1-converted iN cells acquire functional properties of SPN-like cells

Since considerable numbers of DARPP32-positive SPNs are lost after tMCAO (Supplementary Fig. 1A), their regeneration is paramount for adequate functional recovery. When we performed immunostaining with an antibody for DARPP32, the DARPP32-negative area and volume decreased in ND1-treated striatum after tMCAO compared with control (Fig. 2A and B), suggesting that ND1 transduction could repopulate a subtype of cells expressing the SPN-specific marker in the injured striatum.

Next, we asked whether ND1-converted iN cells are indeed functionally integrated into brain circuits as SPN-like cells. When assessed at 4 weeks after CD68–ND1–P2A–EGFP lentivirus injection into the striatum of tMCAO mice, 70% of ND1-transduced cells had become positive for DARPP32 (Fig. 2C and D). ND1-converted iN cells in the striatum also expressed Ctip2, which controls the maturation and survival of SPNs,[39] whereas these cells did not express Cux1 (a marker for cortical neurons) or calretinin (a marker for interneurons) (Supplementary Fig. 4A and B). We also performed patch-clamp recordings of iN cells in the striatum and observed spontaneous action potential firing following depolarization under the current-clamp condition, whereas control virus-infected microglia/macrophages lacked such firing (Fig. 2E and F, and Supplementary Fig. 5A and B). Furthermore, iN cells showed long latencies of spike generation in response to current pulse injections (Supplementary Fig. 5C), consistent with the behaviour of typical SPNs.[40, 41] The median resting membrane potential of iN cells (–87.9 ± 5.5 mV) was similar to what is typical for SPNs,[42-45] whereas iN cells had higher mean input resistance (537 ± 71 MΩ) and slightly lower mean whole-cell capacitance (90.3 ± 11.9 pF) compared to typical SPNs (Supplementary Fig. 5A and D). Moreover, the input resistance of iN cells varied widely, ranging from 180 to 950 MΩ. We also detected spontaneous synaptic events, both excitatory and inhibitory, in iN cells (Fig. 2G), in

contrast with control virus-infected microglia/macrophages (Supplementary Fig. 5E). The frequency and amplitude with these iN cells were similar to those with iN cells in the intact mice.[26] These data suggest that microglia/macrophages were converted into functional iN cells, although not all iN cells had fully matured by 4 weeks after viral injection, in agreement with a previous report.[46]

We then investigated how many microglia/macrophages were converted into iN cells in the injured area and maintained for a long period after tMCAO (Fig. 3A). We employed Cre-inducible diphtheria toxin receptor (iDTR) transgenic mice. Cre-transduced cells in iDTR mice permanently express DTR, even after neuronal conversion, which enables us to trace as well as ablate iN cells. We injected CD68–ND1–P2A–Cre lentivirus into the striatum of iDTR mice at 1 week after tMCAO and traced at two different time points (1 wpi and 8 wpi). Although iN cells were detected at 2 wpi (Fig. 1C and D), almost no DTR and βIII-tubulin double-positive iN cells were observed at 1 wpi (Fig. 3B upper panels and C), indicating that ND1-transduced cells had not yet converted into iN cells at this early time point. Furthermore, there were about 20,000 Iba1/DTR-double-positive cells in total (88% among total DTR-positive cells) in the lesion site at 1 wpi, whereas there were about 2,700 DTR-positive other cell types (12% among total DTR-positive cells) (Fig. 3C). Moreover, although only a small fraction of Iba1/DTR-

double-positive microglia/macrophages expressed Ki67 (a marker for cell proliferation), no or almost no other DTR-positive cells including GFAP-positive astrocytes and APC-positive oligodendrocytes did so (Supplementary Fig. 6A–E), leading us to conclude that the majority of the iN cells were derived from the 20,000 Iba1/DTR-double-positive microglia/macrophages and not from the 2,700 Iba1-negative/DTR-positive non-microglial/macrophage proliferating cells.

Among microglia/macrophages residing in the area depleted of neurons, 5% were infected with ND1 lentivirus and expressed both DTR and Iba1 at 1 wpi (Fig. 3D and E). The lineage-tracing experiment revealed that about 60% of ND1-transduced cells were consequently converted into DARPP32-positive iN cells and maintained in the injured striatum until at least 8 wpi (Fig. 3B lower panels and F). The expression, if any, of βIII-tubulin in mature SPNs is very low compared to that in immature neurons generated from NSCs in the SVZ.[47] In agreement with this, almost all iN cells at 8 wpi exhibited no or very little expression of βIII-tubulin (Supplementary Fig. 7A–D), even though iN cells at 2 wpi were clearly expressing βIII-tubulin (Fig. 1C and D), indicating that iN cells had become more mature SPN-like cells by 8 wpi. The total number of iN cells in the striatum was about 13,000 at 8 wpi (Fig. 3C), a level at which functional recovery of tMCAO mice can be expected by analogy with a previous study of

endogenous NS/PC-derived neurons.[48] Before assessing functional recovery, we checked the anatomical connectivity of iN cells at 8 wpi. The striatum receives projections from dopaminergic neurons in the substantia nigra pars compacta.[49] We used an antibody against the rate-limiting enzyme for dopamine synthesis, tyrosine hydroxylase (TH), which can detect the somas of dopaminergic neurons in the substantia nigra pars compacta and their projections in the striatum. We observed that almost all somas of DARPP32/DTR-double-positive iN cells in the injured striatum contacted TH-positive neuronal processes (Supplementary Fig. 7E and F). In addition, some iN cells were labelled with cholera toxin B (CTB, a retrograde axonal tracer) that had been injected into the globus pallidus, a major target area of SPNs (Fig. 3G and Supplementary Fig. 7G), suggesting that they projected their axons into the globus pallidus in the same way as intrinsic SPNs do.

Together, these results indicate that ND1-converted iN cells were functionally and anatomically integrated into the neural circuitry in the injured brain.

## Neuronal conversion restores functional impairment induced by tMCAO

We next asked whether the neuronal conversion restores behavioural

impairments caused by tMCAO (Fig. 4A). tMCAO mice exhibited asymmetric body movement in the elevated body swing test, corner test, cylinder test and corner rotation, in agreement with previous reports.[30, 48] We found that iN cell generation significantly improved these neurological dysfunctions from 3 wpi (Fig. 4B and Supplementary Video 1–6). The cylinder test demonstrated spontaneous recovery of control virus-injected tMCAO mice. This test is mainly associated with the motor area in the cortex, where almost no neuronal loss is usually incurred by 30-min tMCAO[10, 34] (Fig. 2A). Considering that 90-min tMCAO in mice induces neuronal loss in the cortex in addition to the striatum, and persistently impairs the behaviour associated with the cylinder test,[31] 30-min tMCAO-induced neuronal loss in the striatum only transiently affects the cylinder test,[30] most likely because the cortex is almost intact. Therefore, we did not observe any significant difference between control and ND1 virus-injected tMCAO mice over time. These data indicate that the generation of iN cells in the injured striatum by ND1 improves neurological dysfunctions in the tMCAO mouse model.

## Ablation of iN cells abolishes gained functional recovery

To reveal whether iN cells contribute directly to the recovery, we ablated them using iDTR transgenic mice. We injected CD68–ND1–P2A–Cre lentivirus into the

striatum of iDTR mice after tMCAO and confirmed the dramatic decrease of DTR-positive iN cells following DT administration (Fig. 5A–C). When we ablated iN cells after functional rescue had been observed, the attained recovery was almost completely abolished in ND1-treated tMCAO mice (Fig. 5D). Moreover, when we eliminated ND1- and Cre-transduced cells at 1 week before functional recovery was expected (Fig. 4B), these mice showed no sign of functional recovery (Supplementary Fig. 8), indicating that iN cell maturation in the injured striatum is prerequisite for the recovery. We also investigated whether DT-induced cell death itself exacerbates neurological function, and found that ablation of iN cells in intact mice at 2 wpi (Supplementary Fig. 9A–C) did not affect neurological function (Supplementary Fig. 9D). Thus, these results indicate that iN cells make a direct and major contribution to the functional recovery induced by ND1-mediated direct neuronal conversion of microglia/macrophages.

# Discussion

In this study, we have shown that ND1 enables microglia/macrophages to convert into SPN-like cells, which integrate into existing brain circuits to restore neurological function in the ischaemic area of tMCAO mice. After tMCAO, microglia/macrophages have been shown to exhibit both the classical pro-inflammatory

and the wound-healing reparative anti-inflammatory state. Anti-inflammatory microglia/macrophages increase during 7 days after tMCAO and subside around day 14, whereas pro-inflammatory microglia/macrophages increase and persist until at least day 14.[24, 50] We have previously shown that in addition to microglia in the normal condition, pro-inflammatory microglia induced by lipopolysaccharide stimulation can be converted into iN cells by ND1 transduction.[26] In the present study, we targeted microglia/macrophages residing in the injured area at 1 week after tMCAO by injecting CD68–ND1–P2A–EGFP virus and observed ND1-converted iN cells at 2 wpi (day 21 after MCAO) (Fig. 1C and D), although we found only very few iN cells at 1 wpi (day 14 after MCAO) (Fig. 3B and C). Overall, it seems likely that pro-inflammatory microglia/macrophages are mainly converted into iN cells after tMCAO.

Since pro-inflammatory microglia/macrophages produce pro-inflammatory cytokines and thus induce further damage to CNS tissue, reducing these neurotoxic cells by neuronal conversion may benefit brain repair by increasing the survival of remaining neurons.[51] If this is the case, functional recovery should be retained to some extent, even after the ablation of ND1-transduced cells. However, the recovery attained by neuronal conversion of microglia/macrophages at 3 wpi completely disappeared when we eliminated iN cells at 1 week before functional recovery was expected (Supplementary

Fig. 8B), excluding the above possibility.

Microglia/macrophages provide disease-modifying regulation of various types of cells including astrocytes, oligodendrocytes and leukocytes.[52] In this study, only 5% of microglia/macrophages that converged in the ischemic area were infected by ND1-expressing virus (Fig. 3E). In addition, at 2 wpi, neuronal conversion from microglia/macrophages affected the density of microglia/macrophages only in a very limited area of the injury (Supplementary Fig. 2J). Since this small number of lost microglia/macrophages can be replenished by repopulation from residual microglia[25] or the conversion of peripheral macrophages to microglia-like cells,[18, 19] neuronal conversion from microglia/macrophages causes little exhaustion of the source in the brain and should thus have little adverse effect on the behaviour of other cells after tMCAO.

We found that depletion of microglia-type cells (Tmem119/Iba1-double-positive) by PLX5622 treatment virtually abolished the appearance of ND1-converted iN cells, indicating that the major original cell source converted into iN cells is microglia-type cells and not peripheral macrophage-type cells. However, microglia-like cells originally derived from peripheral macrophages in the lesion area could contribute as a cell source for ND1-mediated neuronal conversion. Although intraperitoneal administration of clodronate liposomes can ablate peripheral macrophages but not

microglia,[53] it remains to be examined whether this microglia-like population can indeed be converted to neurons. After tMCAO, the microglia-like cells and microglia share most microglial markers, including Sall1, a transcriptional regulator defining microglial identity and function.[15, 18] Some homeostatic microglia-specific transcripts that are present in microglia throughout life, but not in liver macrophages during early development or in adult peritoneal macrophages at steady state or after differentiation towards the pro-inflammatory or anti-inflammatory state, have been identified.[19] Among these transcripts, Gpr34 is enriched in microglia compared to peripheral macrophages, even after the macrophages acquire microglia-like identity in the tMCAO brain.[18] Therefore, the development of transgenic mouse lines such as Gpr34-Cre is warranted to distinguish precisely microglia/macrophage subpopulations (i.e., *bona fide* microglia and microglia-like cells derived from infiltrated peripheral macrophages) and to reveal their phenotypic differences in order to indentify the source of iN cells in the ischaemic area.

ND1 is a proneural basic helix-loop-helix transcription factor that is essential for neuronal differentiation from NS/PCs in the CNS. We have previously found that microglia can be directly converted into neurons by expression of this single transcription factor in the intact mouse brain.[26] ND1 penetrates closed chromatin regions associated with bivalent histone modifications (both the active histone mark H3K4me3 and the

repressive mark H3K27me3 simultaneously) in microglia to induce the expression of neuronal genes. These regions are resolved to a monovalent H3K4me3 mark at later stages of reprogramming to establish neuronal identity. Cells such as non-reactive astrocytes that do not retain the bivalent signature in ND1-bound loci around neuronal genes, on the other hand, cannot be reprogrammed by ND1.[26] In the present study, we have shown that ND1 converts microglia/macrophages accumulated in the injured site to neurons; this is probably because these cells have bivalent histone modifications in ND1-bound loci. As we and others have shown, the technology of *in situ* conversion of non-neuronal cells into neurons has opened a new avenue for developing therapeutic strategies for neurological disorders. However, regional and characteristic differences regarding the response to conversion-inducing factors among the original cell source must be taken into account to obtain desired neuronal subtypes effectively. For example, astrocytes in the intact striatum[5] but not in the cortex[4] can be reprogrammed by Sox2. Furthermore, the efficiency of conversion into DARPP32-positive SPN-like cells from astrocytes by ND1 in the striatum is quite low (2%),[54] but can be improved by the combined expression of ND1 with Dlx2.[46] In contrast, expression of ND1 alone in microglia in the same brain region can efficiently induce conversion into DARPP32-positive SPN-like cells (75%).[26] In the present study, we found that striatal microglia/macrophages that have converged in

the ischaemic area can also convert into DARPP32-positive SPN-like cells with high efficiency (70%) (Fig. 2D). These observations suggest that the epigenetic profiles in the original cells and/or external cues from niches in each brain region can determine the response to conversion-inducing transcriptional factors and affect the efficiency of reprogramming to the desired neuronal subtypes. Therefore, although our *in situ* neuronal conversion technology based on ND1 transduction in microglia/macrophages to treat ischaemic injury should be applicable to CNS injuries and diseases other than stroke as long as endogenous microglia/macrophages are available and have bivalent histone modifications in ND1-bound loci, regional variation in the response to conversion-inducing transcriptional factors may limit the efficacy of appropriate iN cell production. In such cases, selection of more suitable conversion-inducing transcription factors than ND1 for region-specific microglia would become essential, warranting further investigation to provide a strategy best matched to each neurological disorder.

We believe our finding, that forced neurogenesis from microglia/macrophages (microglia-type cells) in the injured area through *in vivo* direct reprogramming reinstates neurological function, holds great promise as a therapeutic strategy to treat ischaemic injury and other CNS diseases characterized by neuronal loss, such as traumatic brain injury and spinal cord injury.

# Acknowledgements

We thank H. Nakashima, S. Katada and T. Imamura for discussions; Y. Nakagawa for excellent secretarial assistance; I. Smith for proofreading the manuscript; I. Imayoshi for sharing Nestin-Cre$^{ERT2}$ mice; L. Cong, S. Yeung, P. Singh and A. Rymar (Plexxikon) for providing PLX5622; I. Goto (EPS EKISHIN) for providing the PLX5622-formulated diet; and M. Tachibana, T. Shibahara, T. Ago, Y. Kawamura and N. Kaneko for teaching us how to make and evaluate tMCAO model mice. We appreciate technical assistance from the Research Support Center, Research Center for Human Disease Modeling, Kyushu University Graduate School of Medical Sciences.

# Funding

This work was supported by the Kaibara Morikazu Medical Science Promotion Foundation (to TI), a Grant-in-Aid for Young Scientists (B) JP18K14820 (to TM), the Takeda Science Foundation (to TM), the Qdai-jump Research Program (Wakaba Challenge) of Kyushu University (to TM), a research grant from The Noguchi Institute (to TM), AMED JP21bm0404057 (to TM, KN), the Suzuken Memorial Foundation (to KN), a Grant-in-Aid for Scientific Research on Innovative Areas JP16H06527 (to KN), JP16K21734 (to KN) and a Grant-in-Aid for Challenging Research (Exploratory)

JP19K22473 (to KN).

# Competing interests

The authors report no competing interests.

# Author contributions

TI, TM and KN designed the experiments. TI, TM and YH performed experiments. TI and TM analysed and interpreted the data. TI, TM and KN wrote the manuscript. TM and KN supervised the project. TI, TM and KN acquired funding. AK and JK helped with data acquisition.

# References

1. Niu W, Zang T, Zou Y, et al. In vivo reprogramming of astrocytes to neuroblasts in the adult brain. *Nat Cell Biol*. 2013;15(10):1164-75. doi:10.1038/ncb2843

2. Torper O, Pfisterer U, Wolf DA, et al. Generation of induced neurons via direct conversion in vivo. *Proc Natl Acad Sci U S A*. 2013;110(17):7038-43. doi:10.1073/pnas.1303829110

3. Guo Z, Zhang L, Wu Z, Chen Y, Wang F, Chen G. In vivo direct reprogramming of reactive glial cells into functional neurons after brain injury and in an Alzheimer's disease model. *Cell Stem Cell*. 2014;14(2):188-202. doi:10.1016/j.stem.2013.12.001

4. Heinrich C, Bergami M, Gascon S, et al. Sox2-mediated conversion of NG2 glia into induced neurons in the injured adult cerebral cortex. *Stem Cell Reports*. 2014;3(6):1000-14. doi:10.1016/j.stemcr.2014.10.007

5. Niu W, Zang T, Smith DK, et al. SOX2 reprograms resident astrocytes into neural progenitors in the adult brain. *Stem Cell Reports*. 2015;4(5):780-94. doi:10.1016/j.stemcr.2015.03.006

6. Torper O, Ottosson DR, Pereira M, et al. In Vivo Reprogramming of Striatal NG2 Glia into Functional Neurons that Integrate into Local Host Circuitry. *Cell Rep*. 2015;12(3):474-81. doi:10.1016/j.celrep.2015.06.040

7. Brulet R, Matsuda T, Zhang L, et al. NEUROD1 Instructs Neuronal Conversion in Non-Reactive Astrocytes. *Stem Cell Reports*. 2017;8(6):1506-1515. doi:10.1016/j.stemcr.2017.04.013

8. Chen YC, Ma NX, Pei ZF, et al. A NeuroD1 AAV-Based Gene Therapy for Functional Brain Repair after Ischemic Injury through In Vivo Astrocyte-to-Neuron Conversion. *Mol Ther*. 2020;28(1):217-234. doi:10.1016/j.ymthe.2019.09.003

9. Sommer CJ. Ischemic stroke: experimental models and reality. *Acta Neuropathol*. 2017;133(2):245-261. doi:10.1007/s00401-017-1667-0

10. Buscemi L, Price M, Bezzi P, Hirt L. Spatio-temporal overview of neuroinflammation in an experimental mouse stroke model. *Sci Rep*. 2019;9(1):507. doi:10.1038/s41598-018-36598-4

11. Ginhoux F, Greter M, Leboeuf M, et al. Fate mapping analysis reveals that adult microglia derive from primitive macrophages. *Science*. 2010;330(6005):841-5. doi:10.1126/science.1194637

12. Kierdorf K, Erny D, Goldmann T, et al. Microglia emerge from erythromyeloid precursors via Pu.1- and Irf8-dependent pathways. *Nat Neurosci*. 2013;16(3):273-80. doi:10.1038/nn.3318

13. Gomez Perdiguero E, Klapproth K, Schulz C, et al. Tissue-resident macrophages

originate from yolk-sac-derived erythro-myeloid progenitors. *Nature*. 2015;518(7540):547-51. doi:10.1038/nature13989

14. Hoeffel G, Chen J, Lavin Y, et al. C-Myb(+) erythro-myeloid progenitor-derived fetal monocytes give rise to adult tissue-resident macrophages. *Immunity*. 2015;42(4):665-78. doi:10.1016/j.immuni.2015.03.011

15. Buttgereit A, Lelios I, Yu X, et al. Sall1 is a transcriptional regulator defining microglia identity and function. *Nat Immunol*. 2016;17(12):1397-1406. doi:10.1038/ni.3585

16. Bennett FC, Bennett ML, Yaqoob F, et al. A Combination of Ontogeny and CNS Environment Establishes Microglial Identity. *Neuron*. 2018;98(6):1170-1183 e8. doi:10.1016/j.neuron.2018.05.014

17. Shemer A, Grozovski J, Tay TL, et al. Engrafted parenchymal brain macrophages differ from microglia in transcriptome, chromatin landscape and response to challenge. *Nat Commun*. 2018;9(1):5206. doi:10.1038/s41467-018-07548-5

18. Rajan WD, Wojtas B, Gielniewski B, Gieryng A, Zawadzka M, Kaminska B. Dissecting functional phenotypes of microglia and macrophages in the rat brain after transient cerebral ischemia. *Glia*. 2019;67(2):232-245. doi:10.1002/glia.23536

19. Grassivaro F, Menon R, Acquaviva M, et al. Convergence between Microglia and

Peripheral Macrophages Phenotype during Development and Neuroinflammation. *J Neurosci*. 2020;40(4):784-795. doi:10.1523/JNEUROSCI.1523-19.2019

20. Price CJ, Wang D, Menon DK, et al. Intrinsic activated microglia map to the peri-infarct zone in the subacute phase of ischemic stroke. *Stroke*. 2006;37(7):1749-53. doi:10.1161/01.STR.0000226980.95389.0b

21. Gulyas B, Toth M, Schain M, et al. Evolution of microglial activation in ischaemic core and peri-infarct regions after stroke: a PET study with the TSPO molecular imaging biomarker [((11))C]vinpocetine. *J Neurol Sci*. 2012;320(1-2):110-7. doi:10.1016/j.jns.2012.06.026

22. Annunziato L, Boscia F, Pignataro G. Ionic transporter activity in astrocytes, microglia, and oligodendrocytes during brain ischemia. *J Cereb Blood Flow Metab*. 2013;33(7):969-82. doi:10.1038/jcbfm.2013.44

23. Fumagalli S, Perego C, Pischiutta F, Zanier ER, De Simoni MG. The ischemic environment drives microglia and macrophage function. *Front Neurol*. 2015;6:81. doi:10.3389/fneur.2015.00081

24. Wattananit S, Tornero D, Graubardt N, et al. Monocyte-Derived Macrophages Contribute to Spontaneous Long-Term Functional Recovery after Stroke in Mice. *J Neurosci*. 2016;36(15):4182-95. doi:10.1523/JNEUROSCI.4317-15.2016

25. Huang Y, Xu Z, Xiong S, et al. Repopulated microglia are solely derived from the proliferation of residual microglia after acute depletion. *Nat Neurosci*. 2018;21(4):530-540. doi:10.1038/s41593-018-0090-8

26. Matsuda T, Irie T, Katsurabayashi S, et al. Pioneer Factor NeuroD1 Rearranges Transcriptional and Epigenetic Profiles to Execute Microglia-Neuron Conversion. *Neuron*. 2019;101(3):472-485 e7. doi:10.1016/j.neuron.2018.12.010

27. Hara H, Huang PL, Panahian N, Fishman MC, Moskowitz MA. Reduced brain edema and infarction volume in mice lacking the neuronal isoform of nitric oxide synthase after transient MCA occlusion. *J Cereb Blood Flow Metab*. 1996;16(4):605-11. doi:10.1097/00004647-199607000-00010

28. Percie du Sert N, Alfieri A, Allan SM, et al. The IMPROVE Guidelines (Ischaemia Models: Procedural Refinements Of in Vivo Experiments). *J Cereb Blood Flow Metab*. 2017;37(11):3488-3517. doi:10.1177/0271678X17709185

29. Borlongan CV, Sanberg PR. Elevated body swing test: a new behavioral parameter for rats with 6-hydroxydopamine-induced hemiparkinsonism. *J Neurosci*. 1995;15(7 Pt 2):5372-8.

30. Balkaya M, Krober J, Gertz K, Peruzzaro S, Endres M. Characterization of long-term functional outcome in a murine model of mild brain ischemia. *J Neurosci Methods*.

2013;213(2):179-87. doi:10.1016/j.jneumeth.2012.12.021

31. Li X, Blizzard KK, Zeng Z, DeVries AC, Hurn PD, McCullough LD. Chronic behavioral testing after focal ischemia in the mouse: functional recovery and the effects of gender. *Exp Neurol*. 2004;187(1):94-104. doi:10.1016/j.expneurol.2004.01.004

32. Iqbal AJ, McNeill E, Kapellos TS, et al. Human CD68 promoter GFP transgenic mice allow analysis of monocyte to macrophage differentiation in vivo. *Blood*. 2014;124(15):e33-e44. doi:10.1182/blood-2014-04-568691

33. Hayashi Y, Morinaga S, Zhang J, et al. BK channels in microglia are required for morphine-induced hyperalgesia. *Nat Commun*. 2016;7(1):11697. doi:10.1038/ncomms11697

34. Denes A, Vidyasagar R, Feng J, et al. Proliferating resident microglia after focal cerebral ischaemia in mice. *J Cereb Blood Flow Metab*. 2007;27(12):1941-53. doi:10.1038/sj.jcbfm.9600495

35. Bennett ML, Bennett FC, Liddelow SA, et al. New tools for studying microglia in the mouse and human CNS. *Proc Natl Acad Sci U S A*. 2016;113(12):E1738-46. doi:10.1073/pnas.1525528113

36. Jin WN, Shi SX, Li Z, et al. Depletion of microglia exacerbates postischemic

inflammation and brain injury. *J Cereb Blood Flow Metab*. 2017;37(6):2224-2236. doi:10.1177/0271678X17694185

37. Hilla AM, Diekmann H, Fischer D. Microglia Are Irrelevant for Neuronal Degeneration and Axon Regeneration after Acute Injury. *J Neurosci*. 2017;37(25):6113-6124. doi:10.1523/JNEUROSCI.0584-17.2017

38. Arvidsson A, Collin T, Kirik D, Kokaia Z, Lindvall O. Neuronal replacement from endogenous precursors in the adult brain after stroke. *Nat Med*. 2002;8(9):963-70. doi:10.1038/nm747

39. Arlotta P, Molyneaux BJ, Jabaudon D, Yoshida Y, Macklis JD. Ctip2 controls the differentiation of medium spiny neurons and the establishment of the cellular architecture of the striatum. *J Neurosci*. 2008;28(3):622-32. doi:10.1523/JNEUROSCI.2986-07.2008

40. Kita T, Kita H, Kitai ST. Passive electrical membrane properties of rat neostriatal neurons in an in vitro slice preparation. *Brain Res*. 1984;300(1):129-39. doi:10.1016/0006-8993(84)91347-7

41. Kawaguchi Y, Wilson CJ, Emson PC. Intracellular recording of identified neostriatal patch and matrix spiny cells in a slice preparation preserving cortical inputs. *J Neurophysiol*. 1989;62(5):1052-68. doi:10.1152/jn.1989.62.5.1052

42. Ade KK, Janssen MJ, Ortinski PI, Vicini S. Differential tonic GABA conductances in striatal medium spiny neurons. *J Neurosci*. 2008;28(5):1185-97. doi:10.1523/JNEUROSCI.3908-07.2008

43. Gertler TS, Chan CS, Surmeier DJ. Dichotomous anatomical properties of adult striatal medium spiny neurons. *J Neurosci*. 2008;28(43):10814-24. doi:10.1523/JNEUROSCI.2660-08.2008

44. Ibanez-Sandoval O, Tecuapetla F, Unal B, Shah F, Koos T, Tepper JM. Electrophysiological and morphological characteristics and synaptic connectivity of tyrosine hydroxylase-expressing neurons in adult mouse striatum. *J Neurosci*. 2010;30(20):6999-7016. doi:10.1523/JNEUROSCI.5996-09.2010

45. Willett JA, Cao J, Dorris DM, Johnson AG, Ginnari LA, Meitzen J. Electrophysiological Properties of Medium Spiny Neuron Subtypes in the Caudate-Putamen of Prepubertal Male and Female Drd1a-tdTomato Line 6 BAC Transgenic Mice. *eNeuro*. 2019;6(2):ENEURO.0016–19. doi:10.1523/ENEURO.0016-19.2019

46. Wu Z, Parry M, Hou XY, et al. Gene therapy conversion of striatal astrocytes into GABAergic neurons in mouse models of Huntington's disease. *Nat Commun*. 2020;11(1):1105. doi:10.1038/s41467-020-14855-3

47. Menezes JR, Luskin MB. Expression of neuron-specific tubulin defines a novel

population in the proliferative layers of the developing telencephalon. *J Neurosci*. Sep 1994;14(9):5399-416. doi:10.1523/JNEUROSCI.14-09-05399.1994

48. Kaneko N, Herranz-Perez V, Otsuka T, et al. New neurons use Slit-Robo signaling to migrate through the glial meshwork and approach a lesion for functional regeneration. *Sci Adv*. 2018;4(12):eaav0618. doi:10.1126/sciadv.aav0618

49. Niu W, Zang T, Wang LL, Zou Y, Zhang CL. Phenotypic Reprogramming of Striatal Neurons into Dopaminergic Neuron-like Cells in the Adult Mouse Brain. *Stem Cell Reports*. 2018;11(5):1156-1170. doi:10.1016/j.stemcr.2018.09.004

50. Hu X, Li P, Guo Y, et al. Microglia/macrophage polarization dynamics reveal novel mechanism of injury expansion after focal cerebral ischemia. *Stroke*. 2012;43(11):3063-70. doi:10.1161/STROKEAHA.112.659656

51. Gascon S, Masserdotti G, Russo GL, Gotz M. Direct Neuronal Reprogramming: Achievements, Hurdles, and New Roads to Success. *Cell Stem Cell*. 2017;21(1):18-34. doi:10.1016/j.stem.2017.06.011

52. Greenhalgh AD, David S, Bennett FC. Immune cell regulation of glia during CNS injury and disease. *Nat Rev Neurosci*. 2020;21(3):139-152. doi:10.1038/s41583-020-0263-9

53. Schmidt A, Strecker JK, Hucke S, et al. Targeting Different Monocyte/Macrophage

Subsets Has No Impact on Outcome in Experimental Stroke. *Stroke*. 2017;48(4):1061-1069. doi:10.1161/STROKEAHA.116.015577

54. Liu MH, Li W, Zheng JJ, Xu YG, He Q, Chen G. Differential neuronal reprogramming induced by NeuroD1 from astrocytes in grey matter versus white matter. *Neural Regen Res*. 2020;15(2):342-351. doi:10.4103/1673-5374.265185

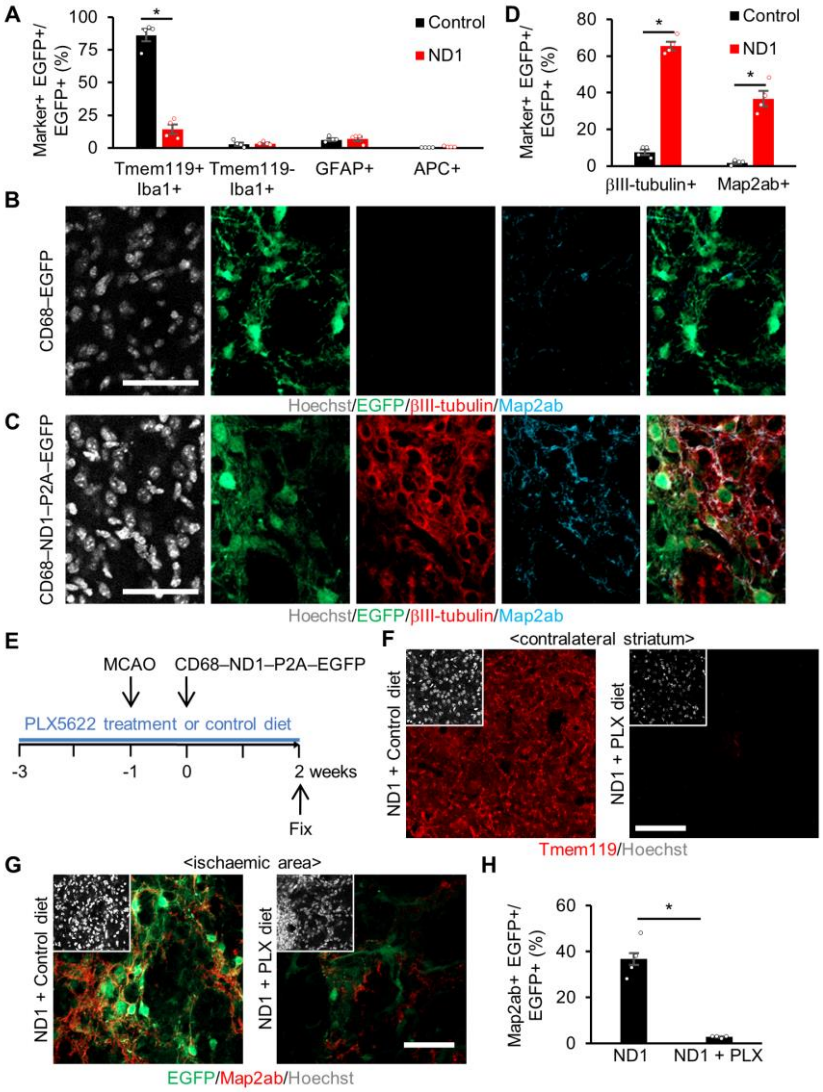


**Figure 1 ND1 programs neuronal conversion from microglia/macrophages in the ischaemic striatum.** (**A**) Quantification of the indicated marker-positive cells in the striatum at 2 wpi ($n = 4$ per group). * $P < 0.05$, two-tailed Mann–Whitney U test. (**B, C**) Representative images of staining for EGFP (green)-, βIII-tubulin (red)- and Map2ab (cyan)-positive cells in the ischaemic area of control (**B**) and ND1 (**C**) virus-treated mice at 2 wpi. Scale bars, 50 μm. (**D**) Quantification of the indicated marker-positive cells in (**B**) and (**C**) ($n = 4$ per group). * $P < 0.05$, two-tailed Mann–Whitney U test. (**E**) Schematic

representation of microglial depletion from the brain. (**F**) Representative images of staining for Tmem119 (red) in the striatum contralateral to the lesion in tMCAO mice treated with control or PLX diets at 2 wpi. Scale bar, 50 μm. (**G**) Representative images of staining for EGFP (green) and Map2ab (red) in the ischaemic area of the striatum in tMCAO mice treated with control or PLX diets at 2 wpi. Scale bar, 50 μm. (**H**) Quantification of the indicated marker-positive cells in (**G**) ($n = 4$ per group). * $P < 0.05$, two-tailed Mann–Whitney U test.

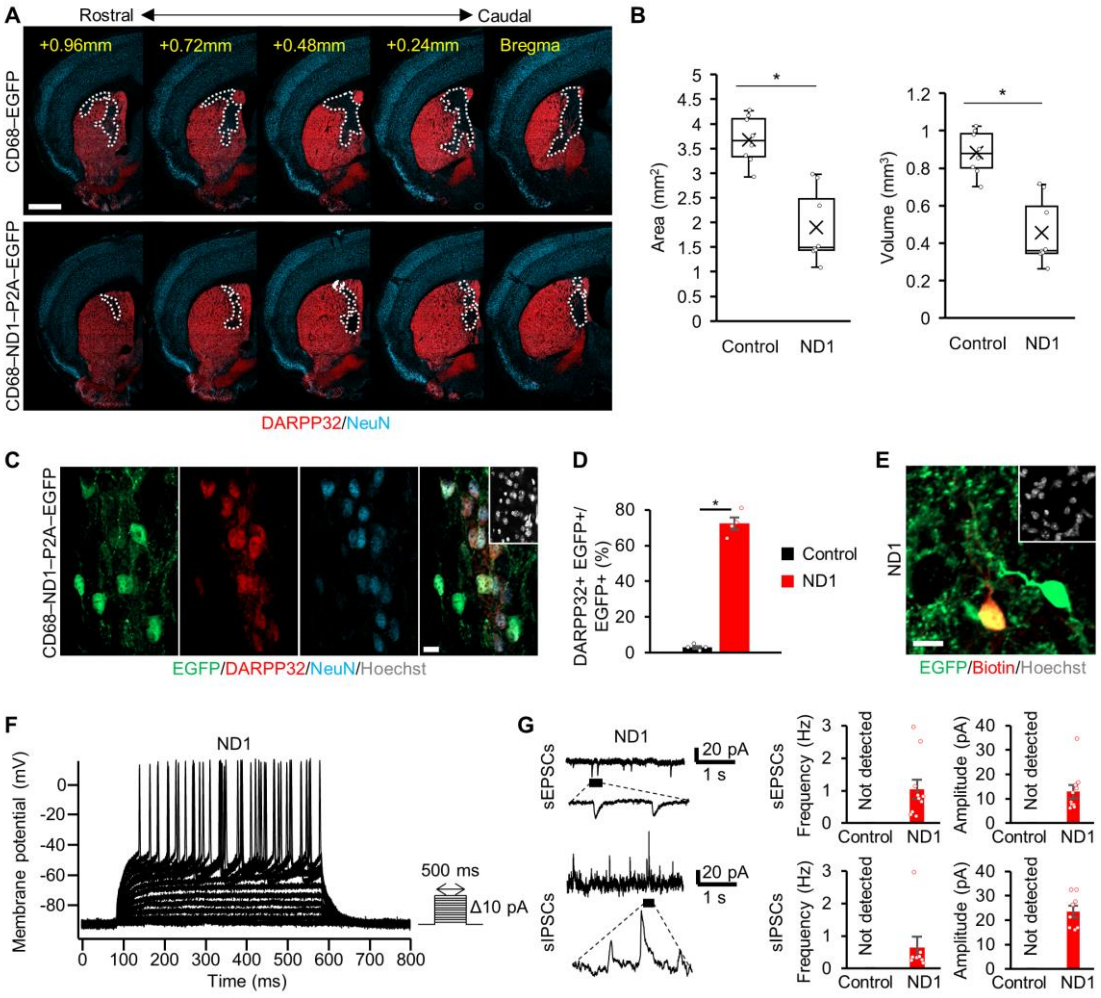


**Figure 2 ND1 converts microglia/macrophages into SPN-like cells in the ischaemic striatum.** (**A**) Representative images of staining for DARPP32 (red) and NeuN (cyan) in control and ND1 virus-treated ischaemic hemispheres from bregma to 0.96 mm rostral at 8 wpi. White dashed enclosures show the DARPP32-negative area in the striatum. Scale bar, 1 mm. (**B**) Quantification of DARPP32-negative area (left) and volume (right) in the striatum within the range from bregma to 0.96 mm rostral ($n$ = 8 per group). * $P < 0.05$, two-tailed Mann–Whitney U test. (**C**) Representative images of staining for EGFP (green), DARPP32 (red) and NeuN (cyan) in ND1 virus-injected striatum at 4 wpi. Scale bar, 10

μm. (**D**) Percentage of DARPP32-positive cells among EGFP-positive cells in control or ND1 virus-treated ischaemic regions at 4 wpi ($n$ = 4 per group). * $P < 0.05$, two-tailed Mann–Whitney U test. (**E**) Representative image of a recorded EGFP-positive iN cell labelled with biotin at 4 weeks after ND1 transduction. Scale bar, 10 μm. (**F**) Representative traces of spontaneous firing activity of action potentials by the depolarizing current steps in an iN cell in the striatum under the current-clamp condition. The inset indicates the configuration of step-pulses elicited from the patch pipette (cumulative step stimulation from the resting potential with 10 pA for 500 ms duration). (**G**) Representative traces of spontaneous excitatory postsynaptic currents (sEPSCs) and spontaneous inhibitory postsynaptic currents (sIPSCs) recorded from iN cells, and bar graphs showing the frequency (left) and amplitude (right) of sEPSCs of control ($n$ = 11 cells from 3 animals) and iN ($n$ = 10 cells from 3 animals) cells and sIPSCs of control ($n$ = 11 cells from 3 animals) and iN ($n$ = 8 cells from 3 animals) cells in the striatum under the voltage-clamp condition.

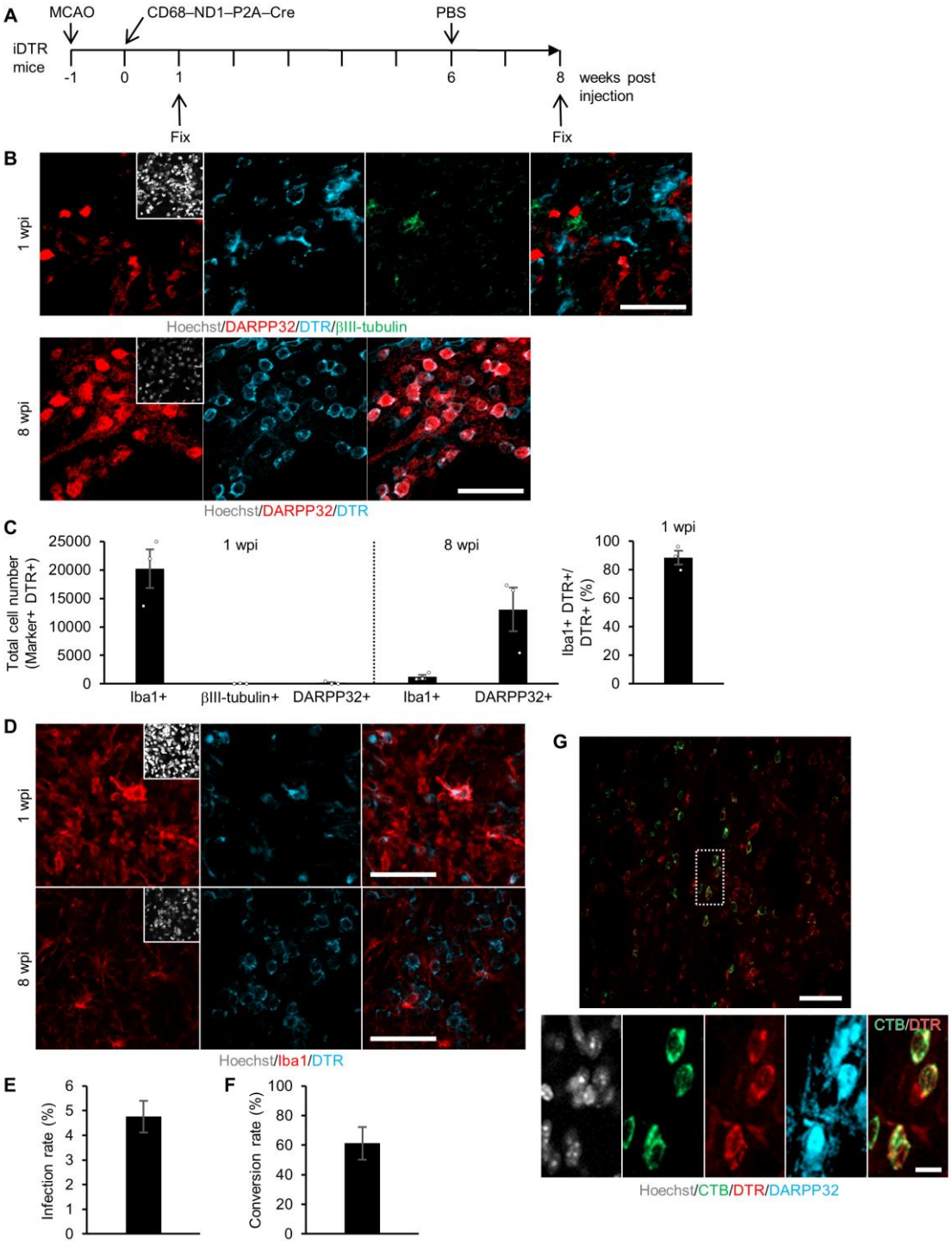


**Figure 3 iN cells survive in the injured region and project their axons into the globus pallidus.** (**A**) Schematic representation of infected microglia/macrophages at 1 wpi and iN cells at 8 wpi in tMCAO mice injected with CD68–ND1–P2A–Cre lentivirus into the

striatum. (**B**) Representative images of staining for DARPP32 (red), DTR (cyan) and βIII-tubulin (green) in the ischaemic area of ND1–P2A–Cre virus-injected striatum at 1 wpi or staining for DARPP32 (red) and DTR (cyan) in the ischaemic area of ND1–P2A–Cre virus-injected striatum at 8 wpi. Scale bars, 50 μm. (**C**) Quantification of the indicated marker-positive cells in the virus-injected area of the striatum ($n$ = 3 per group). (**D**) Representative images of staining for Iba1 (red) and DTR (cyan) in the ischaemic area of ND1–P2A–Cre virus-injected striatum at 1 or 8 wpi. Scale bar, 50 μm. (**E**) Infection rate of microglia/macrophages following virus injection into the striatum ($n$ = 3 per group). (**F**) Neuronal conversion rate of microglia/macrophages in the striatum ($n$ = 3 per group). (**G**) Representative images of staining for CTB (green), DTR (red) and DARPP32 (cyan) in the striatum of iDTR tMCAO model mice administered PBS. The mice were injected with CTB into the globus pallidus at 10 weeks after CD68–ND1–P2A–Cre lentivirus injection. The lower image group comprises magnified views of the white dashed box in the upper panel. Scale bars, 50 μm (upper), 10 μm (lower).

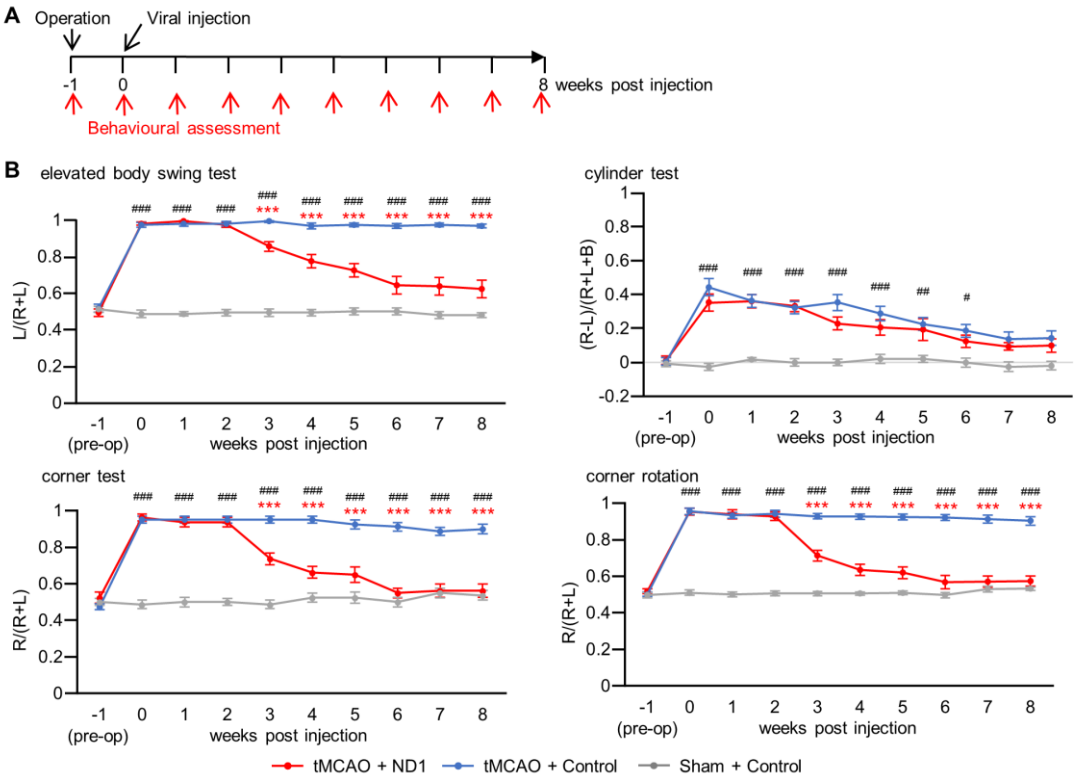


**Figure 4 ND1-mediated microglia/macrophage-to-neuron conversion restores functional impairment after tMCAO.** (**A**) Experimental timeline to investigate the functional recovery of tMCAO mice. (**B**) Time course of changes in scores in the elevated body swing test, cylinder test, corner test and corner rotation test as indicated. Red lines, ND1 virus-treated tMCAO (tMCAO + ND1) group; blue lines, control virus-treated tMCAO (tMCAO + Control) group; grey lines, control virus-infected sham operation (Sham + Control) group ($n$ = 8 per group). *** $P < 0.001$, two-way repeated-measures ANOVA, *post hoc* Bonferroni's multiple comparison test for tMCAO + ND1 vs tMCAO + Control. $^{\#}P < 0.05$, $^{\#\#}P < 0.01$, $^{\#\#\#}P < 0.001$, two-way repeated-measures ANOVA, *post hoc* Bonferroni's multiple comparison test for tMCAO + Control vs Sham + Control.

1 See also Supplementary Videos 1 to 6.

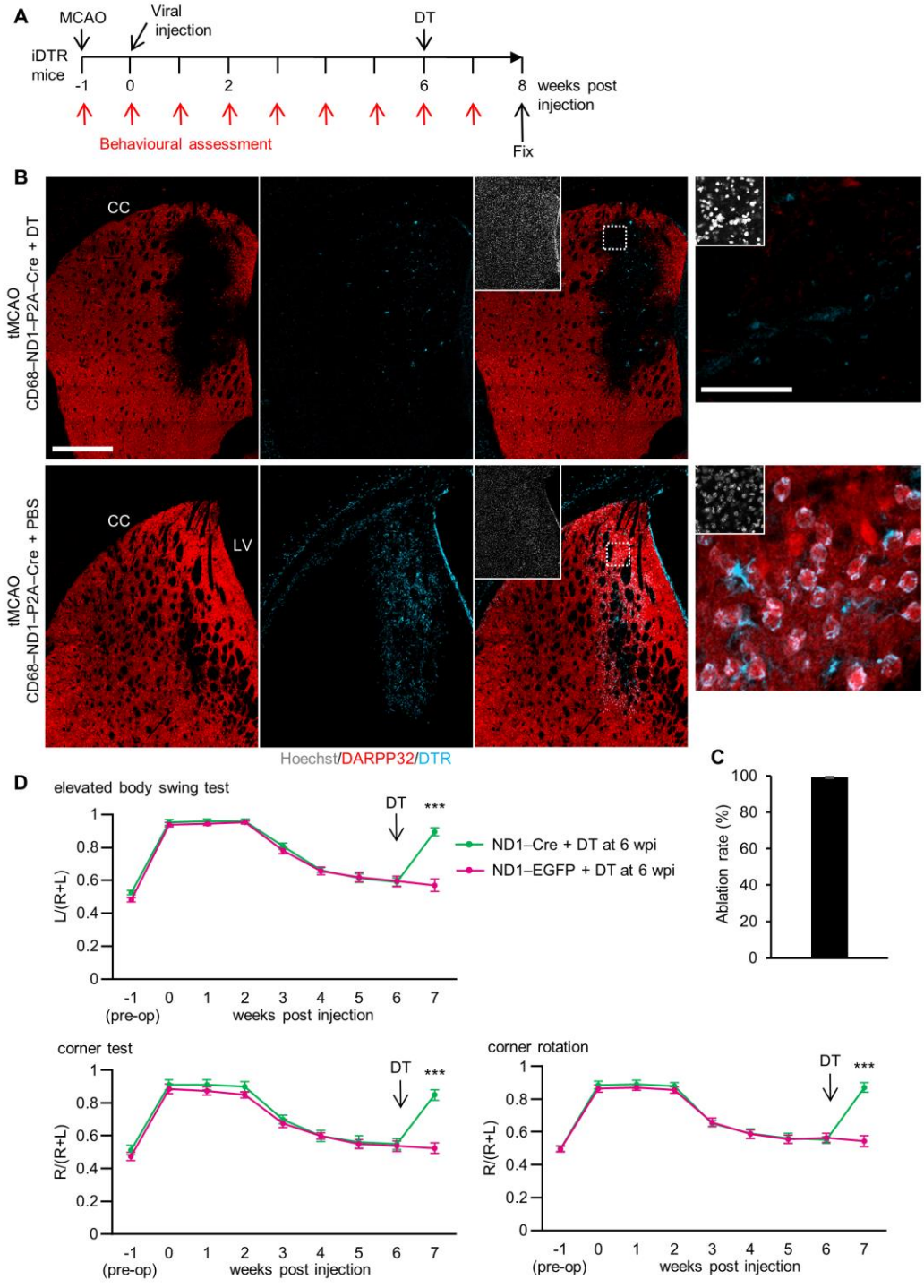


**Figure 5 Ablation of iN cells abolishes gained functional recovery.** (**A**) Schematic representation of the ablation of DTR-expressing cells after functional recovery was observed in tMCAO mice. (**B**) Representative images of staining for DARPP32 (red) and

DTR (cyan) in the striatum of iDTR mice administered DT or PBS. Each rightmost panel is a magnified view of the white square in the panel to its left. Scale bars, 500 μm (left), 50 μm (right). CC, corpus callosum. LV, lateral ventricle. (**C**) Ablation rate of iN cells following DT administration in the virus-injected area of the striatum ($n$ = 3 per group). (**D**) Time course of changes in scores in the indicated tests. iDTR tMCAO model mice were administered DT intraperitoneally at 6 weeks after CD68–ND1–P2A–Cre (green line, ND1–Cre + DT at 6 wpi, $n$ = 8) or CD68–ND1–P2A–EGFP (magenta line, ND1–EGFP + DT at 6 wpi, $n$ = 8) lentiviral injection. *** $P < 0.001$, two-way repeated-measures ANOVA and *post hoc* Bonferroni's multiple comparison test.

# Supplementary Materials

Contents:

neurological function.

## Legends for videos S1 to S6

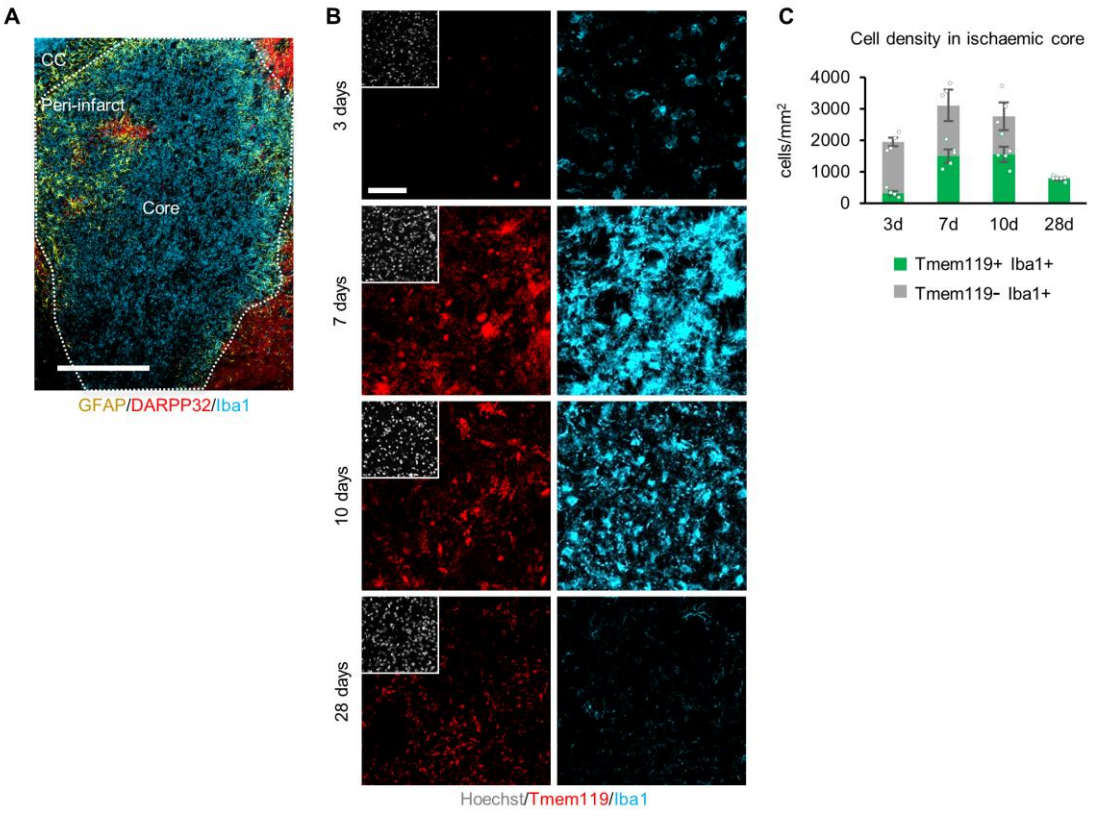


**Supplementary Figure 1. Microglia/macrophages accumulate in the ischaemic core after tMCAO.** (**A**) Representative image of staining for GFAP (yellow), DARPP32 (red) and Iba1 (cyan) in the ischaemic striatum at 7 days after tMCAO. White dashed enclosure shows peri-infarct area. Scale bar, 500 μm. CC, corpus callosum. (**B**) Spatiotemporal distribution of microglia/macrophages after tMCAO. Representative images of staining for Tmem119 (red) and Iba1 (cyan) in the ischaemic core of the striatum at 3, 7, 10 and 28 days after tMCAO. Nuclei were stained with Hoechst. Scale bar, 50 μm. (**C**) Quantification of indicated marker-positive cells in the ischaemic core in (**B**) ($n$ = 4 per

group).

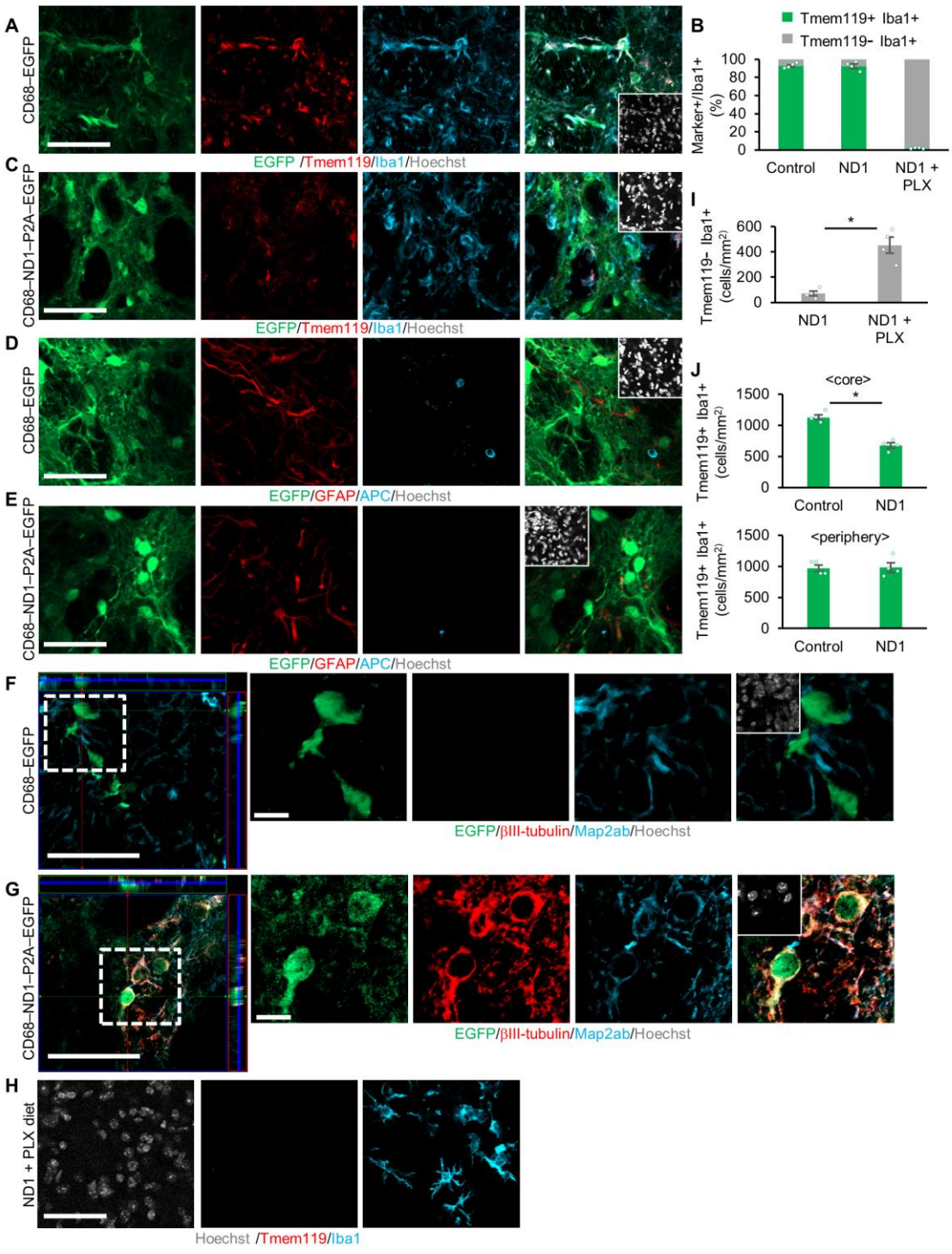


**Supplementary Figure 2. Most cells expressing EGFP under the *CD68* promoter in the ischaemic area are microglia-type cells.** (**A, C**) Representative images of EGFP

(green)-, Tmem119 (red)- and Iba1 (cyan)-positive cells in the ischaemic area of EGFP (control) (**A**) or ND1–P2A–EGFP (**C**) virus-injected striatum at 2 wpi. (**B**) Quantification of indicated marker-positive cells in the virus-injected area of the striatum in (**A**), (**C**) and (**H**) ($n = 4$ per group). (**D, E**) Representative images of staining for EGFP (green), GFAP (red) and APC (cyan) in the ischaemic area of control (**D**) or ND1–P2A–EGFP (**E**) virus-injected striatum at 2 wpi. (**F, G**) Representative images of staining for EGFP (green)-, βIII-tubulin (red)- and Map2ab (cyan)-positive cells in the ischaemic area of control (**F**) and ND1 (**G**) virus-treated mice at 2 wpi. Each right image group comprises magnified views of the white squares in the respective left panels. Scale bars, 50 μm (left), 10 μm (right). (**H**) Representative images of staining for Tmem119 (red) and Iba1 (cyan) in the ischaemic area of the striatum in tMCAO mice treated with PLX diet at 2 wpi. Nuclei were stained with Hoechst. Scale bars, 50 μm. (**I**) Quantification of Tmem119-negative and Iba1-positive macrophages in the virus-injected area of the striatum in (**C**) and (**H**) ($n = 4$ per group). * $P < 0.05$, two-tailed Mann–Whitney U test. (**J**) Quantification of Tmem119- and Iba1-positive microglia-type cells in the virus-injected core (**A**, **C**) and peripheral area of the striatum ($n = 4$ per group respectively). * $P < 0.05$, two-tailed

1 Mann–Whitney U test.

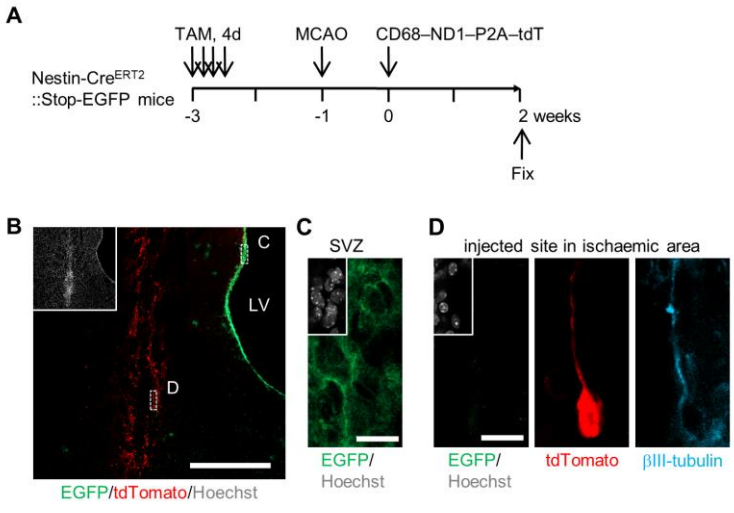


**Supplementary Figure 3. NS/PCs are not the origin of iN cells.** (**A**) Schematic representation of tamoxifen-triggered fate mapping for Nestin-expressing cells before tMCAO. Nestin–Cre$^{ERT2}$::Stop–EGFP mice were given tamoxifen orally for 4 consecutive days, starting at 2 weeks before MCAO, to permanently label Nestin-positive cells and their progeny (**B–D**) Representative images of staining for EGFP (green), tdTomato (red) and βIII-tubulin (cyan) in the ischaemic area of the striatum at 2 wpi. The right panels (**C**) and (**D**) are enlargements of the white dashed boxes C and D, respectively, in the left panel. Scale bars, 500 μm (left), 10 μm (right). LV, lateral ventricle. SVZ, subventricular zone.

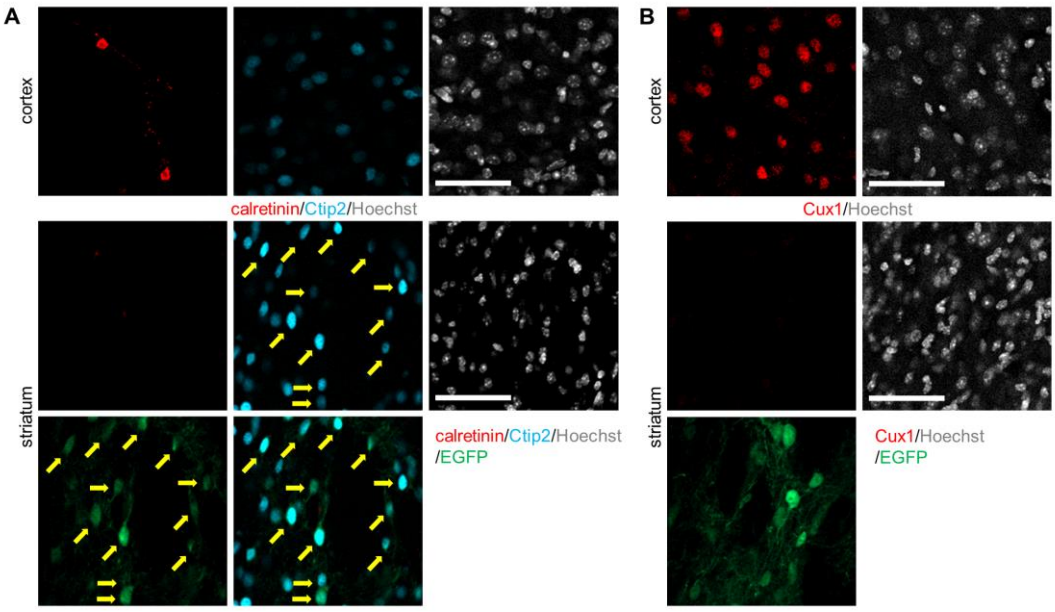


**Supplementary Figure 4. Neuronal marker expression in iN cells.** (**A**) Representative images of staining for EGFP (green), calretinin (red) and Ctip2 (cyan) in the cortex (upper panels) or the ischaemic area of the striatum (lower panels) of ND1 virus-treated mice at 4 wpi. Yellow arrows indicate EGFP- and Ctip2-positive iN cells. Scale bars, 50 μm. (**B**) Representative images of staining for EGFP (green) and Cux1 (red) in the cortex (upper panels) or the ischaemic area of the striatum (lower panels) of ND1 virus-treated mice at 4 wpi. Scale bars, 50 μm.

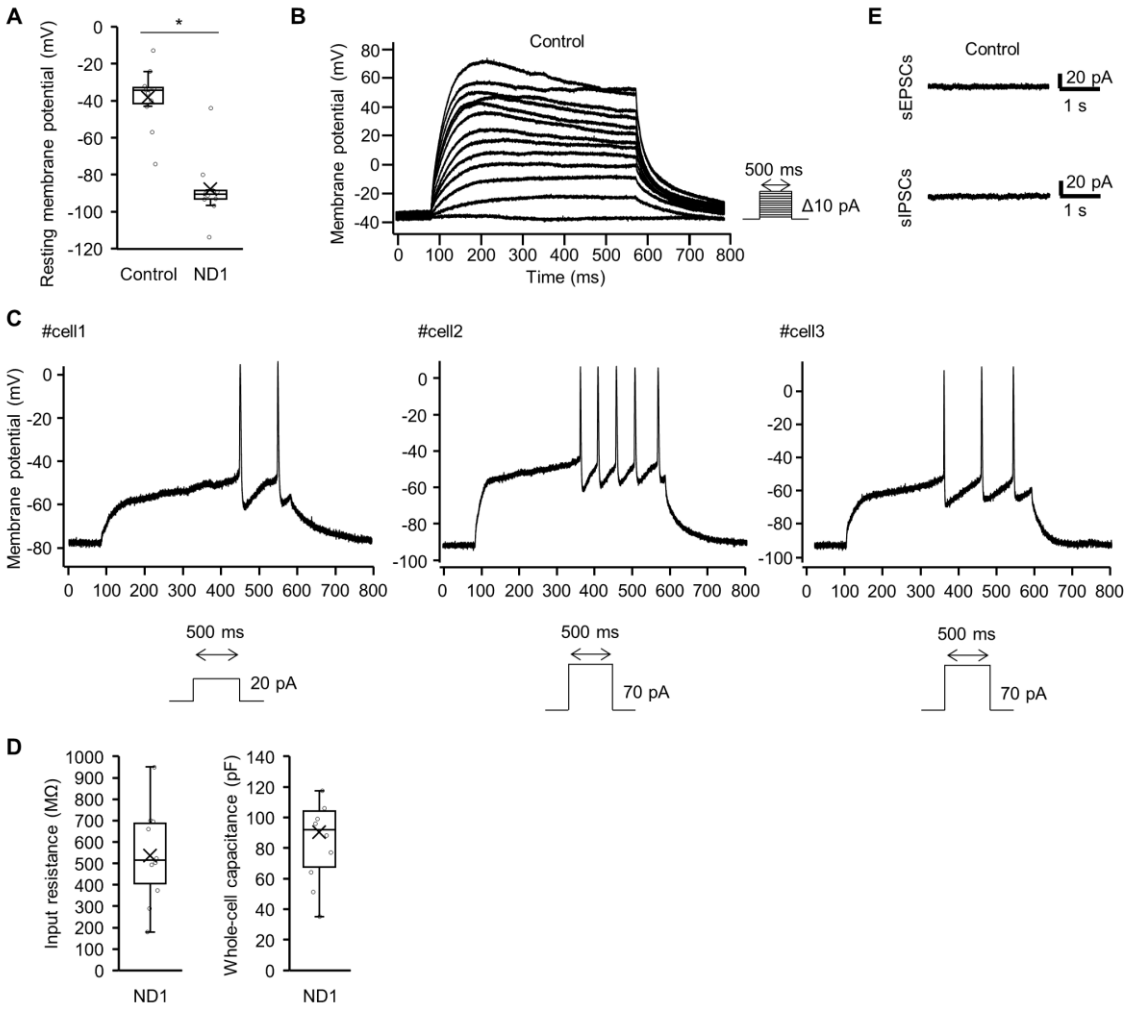


**Supplementary Figure 5. iN cells exhibit neuronal electrophysiological properties.** (**A**) Box-and-whisker plot showing the resting membrane potential of control cells in the striatum at 4 wpi with CD68–EGFP (Control, $n$ = 11 cells from 3 animals) or iN cells in the striatum at 4 wpi with CD68–ND1–P2A–EGFP (ND1, $n$ = 10 cells from 3 animals) lentiviruses. * $P < 0.05$, two-tailed Mann–Whitney U test. (**B**) Representative traces of spontaneous firing activity of action potentials by the depolarizing current steps in a

control cell in the striatum under the current-clamp condition. The inset indicates the configuration of step-pulses elicited from the patch pipette (cumulative step stimulation from the resting potential with 10 pA for 500 ms duration). (**C**) The three sampled iN cells in ND1-treated striatum showed long latencies of spike generation in response to current pulse injections. (**D**) Box-and-whisker plots showing the input resistance and whole-cell capacitance of iN cells in the striatum at 4 wpi with CD68–ND1–P2A–EGFP (ND1, $n$ = 10 cells from 3 animals) lentiviruses. (**E**) Lack of spontaneous excitatory postsynaptic currents (sEPSCs) and spontaneous inhibitory postsynaptic currents (sIPSCs) recorded from a control cell in the striatum under the voltage-clamp condition.

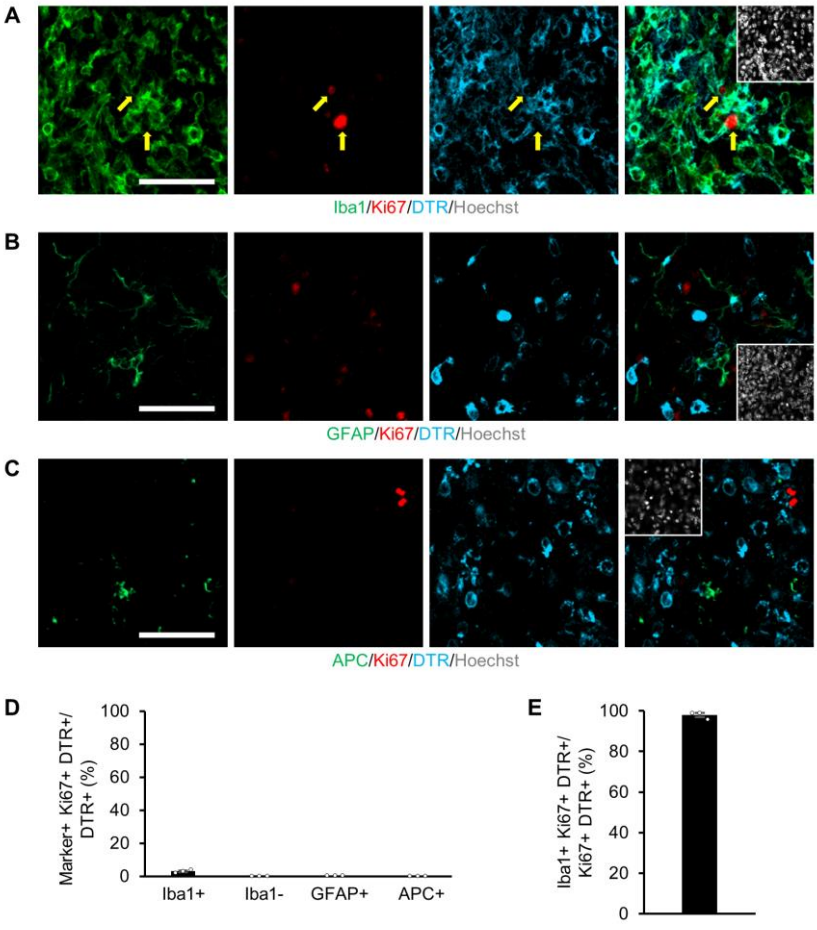


**Supplementary Figure 6. Almost no DTR-positive proliferating cells in the ischemic area.** (**A–C**) Representative images of staining for Iba1 (green; **A**), GFAP (green; **B**), APC (green; **C**), Ki67 (red) and DTR (cyan) in the ischaemic area of ND1–P2A–Cre virus-injected striatum at 1 wpi. Scale bars, 50 μm. Yellow arrows indicate Iba1-, Ki67- and DTR-positive cells. (**D**) Quantification of the indicated marker-positive/negative cells in the ischaemic area of ND1–P2A–Cre virus-injected striatum at 1 wpi ($n$ = 3). (**E**) Percentage of Iba1-, Ki67- and DTR-positive cells among Ki67- and DTR-positive cells

in the ischaemic area of ND1–P2A–Cre virus-injected striatum at 1 wpi ($n$ = 3).

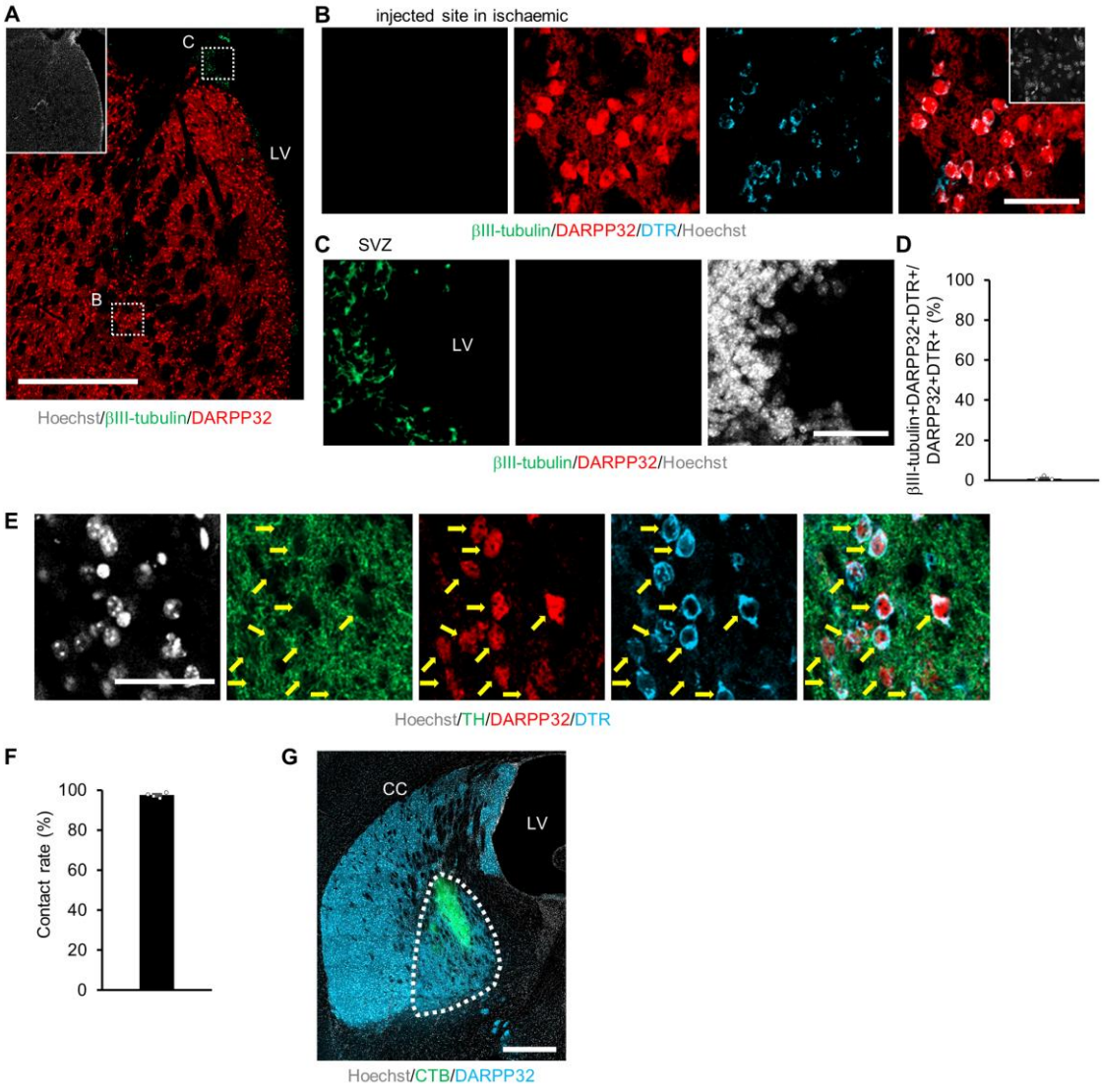


**Supplementary Figure 7. iN cells are integrated into brain circuits in the ischaemic area.** (**A–C**) Representative images of staining for βIII-tubulin (green), DARPP32 (red) and DTR (cyan) in the ischaemic area of ND1–P2A–Cre virus-injected striatum at 8 wpi. The right panels (**B**) and (**C**) are enlargements of the white dashed boxes B and C, respectively, in the leftmost panel. Scale bars, 500 μm (left), 50 μm (right). LV, lateral ventricle. SVZ, subventricular zone. (**D**) Percentage of βIII-tubulin-positive cells among

DARPP32- and DTR-positive cells in the ischaemic area of ND1–P2A–Cre virus-injected striatum at 8 wpi ($n = 3$). (**E**) Representative images of staining for TH (green), DARPP32 (red) and DTR (cyan) in the striatum of iDTR tMCAO model mice administered PBS. Scale bar, 50 μm. Yellow arrows indicate contact between TH-positive neuronal processes and DARPP32- and DTR-positive neuronal somas. (**F**) Quantification of contact between TH-positive neuronal processes and DARPP32- and DTR-positive neuronal somas in the injured striatum ($n = 4$). (**G**) Representative image of staining for CTB (green) and DARPP32 (cyan) in the globus pallidus of iDTR tMCAO model mice administered PBS. White dashed enclosure shows the globus pallidus. Scale bar, 500 μm. CC, corpus callosum. LV, lateral ventricle.

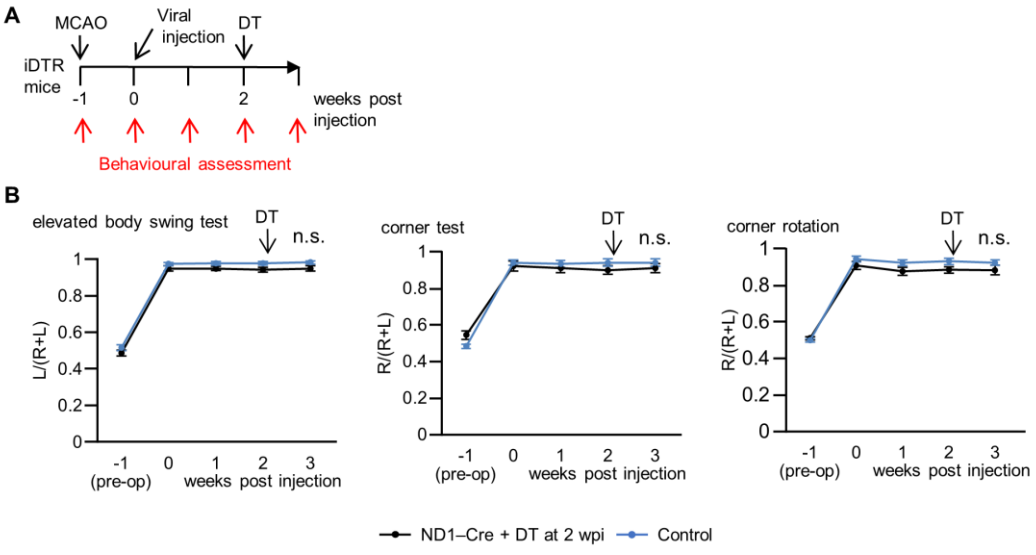


**Supplementary Figure 8. Ablation of ND1 and Cre-transduced cells before functional recovery abolishes expected functional recovery.** (**A**) Schematic representation of the ablation of DTR-expressing cells before functional recovery was observed in tMCAO mice. (**B**) Time course of changes in scores in the elevated body swing test, corner test and corner rotation test. iDTR tMCAO model mice were administered DT intraperitoneally at 2 weeks after CD68–ND1–P2A–Cre lentiviral injection (ND1–Cre + DT at 2 wpi, black line, $n = 9$). Control group consisted of wild-type tMCAO model mice injected with CD68–EGFP (Control, blue line, $n = 12$). n.s., not significant, two-way repeated-measures ANOVA and *post hoc* Bonferroni's multiple comparison test.

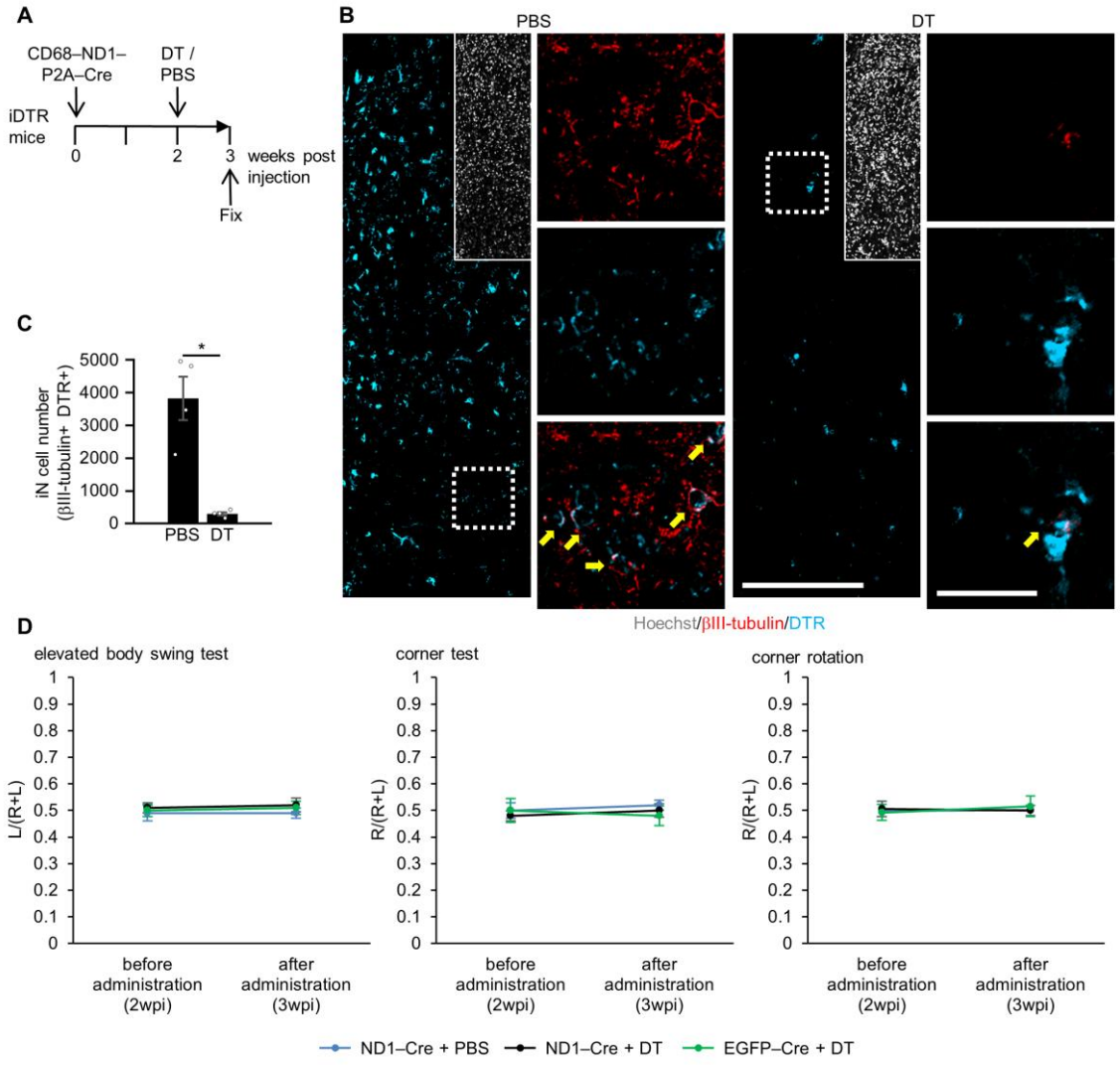


**Supplementary Figure 9. Ablation of iN cells in intact mice does not affect their neurological function.** (**A**) Schematic representation of how we evaluated the efficiency of DTR-expressing iN cell ablation following DT administration. Intact iDTR mice were injected with CD68–ND1–P2A–Cre lentivirus into the striatum. These mice were administered DT or PBS intraperitoneally at 2 wpi. (**B**) Representative images of staining for βIII-tubulin (red) and DTR (cyan) in the striatum of iDTR mice administered PBS or

DT. Each right image group comprises magnified views of the white squares in the respective left panels. Yellow arrows (bottom right) indicate βIII-tubulin- and DTR-positive iN cells. Scale bars, 200 μm (left), 50 μm (right). (**C**) Quantification of iN cell (βIII-tubulin and DTR double-positive) numbers in the virus-injected area of the striatum ($n$ = 4 per group). * $P < 0.05$, two-tailed Mann–Whitney U test. (**D**) Time course of changes in scores in the elevated body swing test, corner test and corner rotation test. Intact iDTR mice were administered DT or PBS intraperitoneally at 2 weeks after CD68–ND1–P2A–Cre, or DT at 2 weeks after CD68–EGFP–P2A–Cre lentiviral injection (ND1–Cre + PBS at 2 wpi, blue line, $n$ = 5; ND1–Cre + DT at 2 wpi, black line, $n$ = 5; EGFP–Cre + DT at 2 wpi, green line, $n$ = 5).

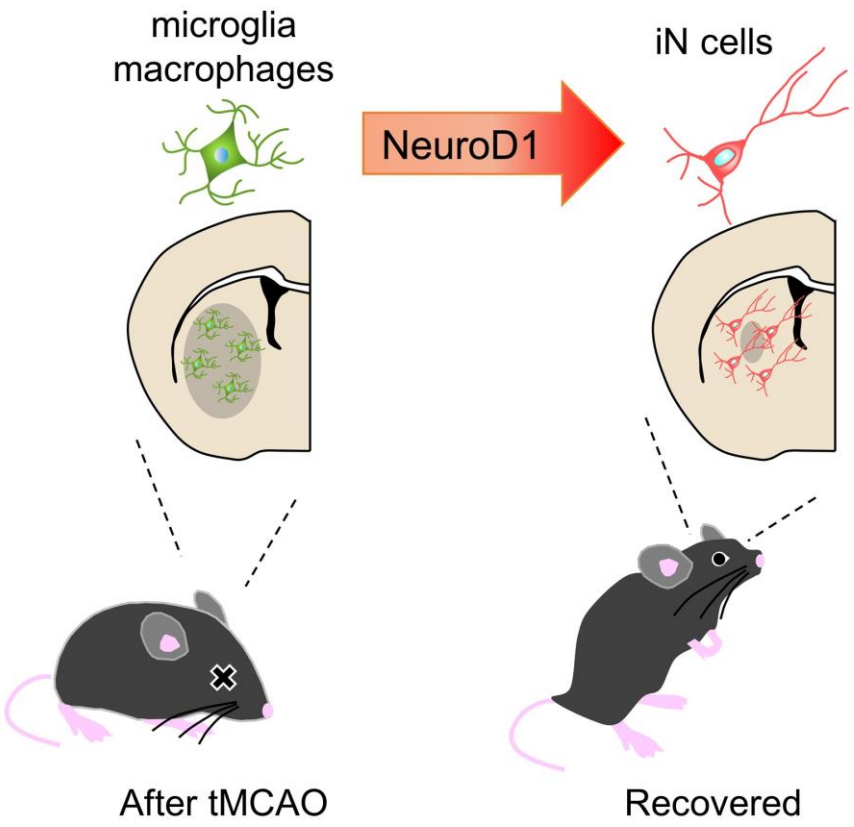


**Thumbnail Figure. A scheme of neurological functional recovery after ischaemic injury though direct cell conversion.**

ND1 enables microglia/macrophages to convert into SPNs in the ischaemic area of tMCAO mice. The neuronal conversion contributes critically to the functional recovery after tMCAO.

**Supplementary Videos**

**Supplementary Video 1. Elevated body swing test in tMCAO + Control mouse at 8 wpi, Related to Fig. 4B.**

**Supplementary Video 2. Elevated body swing test in tMCAO + ND1 mouse at 8 wpi, Related to Fig. 4B.**

**Supplementary Video 3. Elevated body swing test in sham-operated mouse, Related to Fig. 4B.**

**Supplementary Video 4. Corner test and corner rotation in tMCAO + Control mouse at 8 wpi, Related to Fig. 4B.**

**Supplementary Video 5. Corner test and corner rotation in tMCAO + ND1 mouse at 8 wpi, Related to Fig. 4B.**

**Supplementary Video 6. Corner test and corner rotation in sham-operated mouse, Related to Fig. 4B.**